Superseded by NASA TND-842

CONFIDENTIAL

Copy
RM L57I23

NACA

RESEARCH MEMORANDUM

NORMAL-FORCE AND HINGE-MOMENT CHARACTERISTICS AT TRANSONIC SPEEDS OF FLAP-TYPE AILERONS AT THREE SPANWISE LOCATIONS ON A 4-PERCENT-THICK SWEPTBACK-WING—BODY MODEL AND PRESSURE-DISTRIBUTION MEASUREMENTS ON AN INBOARD AILERON

By Jack F. Runckel and Gerald Hieser

Langley Aeronautical Laboratory
Langley Field, Va.

NATIONAL ADVISORY COMMITTEE
FOR AERONAUTICS

WASHINGTON

December 5, 1957

CONFIDENTIAL

NATIONAL ADVISORY COMMITTEE FOR AERONAUTICS

RESEARCH MEMORANDUM

NORMAL-FORCE AND HINGE-MOMENT CHARACTERISTICS AT TRANSONIC SPEEDS OF FLAP-TYPE AILERONS AT THREE SPANWISE LOCATIONS ON A 4-PERCENT-THICK SWEPTBACK-WING—BODY MODEL AND PRESSURE-DISTRIBUTION MEASUREMENTS ON AN INBOARD AILERON

By Jack F. Runckel and Gerald Hieser

SUMMARY

An investigation has been conducted at the Langley 16-foot transonic tunnel to determine the loading characteristics of flap-type ailerons located at inboard, midspan, and outboard positions on a 45° sweptback-wing—body combination. Aileron normal-force and hinge-moment data have been obtained at Mach numbers from 0.80 to 1.03, with angles of attack up to about 27°, and at aileron deflections between approximately ±15°.

Results of the investigation indicate that the loading over the ailerons was established by the wing-flow characteristics, and the loading shapes were irregular in the transonic speed range. The spanwise location of the aileron had little effect on the values of the slope of the curves of hinge-moment coefficient against aileron deflection, but the inboard aileron had the greatest value of the slope of the curves of hinge-moment coefficient against angle of attack and the outboard aileron had the least. Hinge-moment and aileron normal-force data taken with strain-gage instrumentation are compared with data obtained with pressure measurements.

INTRODUCTION

Because of the mixture of subsonic and supersonic flow encountered in the transonic speed range, the prediction of loads on airplane components by theoretical means is difficult. As a result, experimental research is needed to supply loading information. Almost all previous experimental investigations at transonic speeds have been conducted by

utilizing small scale models, with which detailed loads information cannot be obtained. A considerable amount of overall loading information on ailerons at transonic speeds, however, has been obtained on small scale models by the transonic-bump technique. (See, for example, refs.1 and 2.)

As a part of a study in the Langley 16-foot transonic tunnel to obtain information on transonic loads by utilizing larger scale models, the present investigation includes overall loads and load-distribution studies on ailerons installed on a 45° sweptback-wing model. Overall loads were obtained on an inboard, a midspan, and an outboard aileron with strain-gage instrumentation; whereas, load distributions on the inboard aileron were obtained from pressure measurements, and results from these two test techniques are compared. The loading characteristics of an outboard aileron on an unswept-wing model, which was also a part of the aileron-loads study, are reported in reference 3.

The sting-supported model used for the present investigation has a 45° sweptback wing with an aspect ratio of 3, a taper ratio of 0.2, and NACA 65A004 airfoil sections in the streamwise direction. The inboard, midspan, and outboard unbalanced ailerons each have a span of about 40 percent of the wing semispan and a chord of 30 percent of the local wing chord. The longitudinal stability characteristics of this model without ailerons are presented in reference 4, the lateral effectiveness characteristics of the ailerons are given in reference 5, and the loading on the wing and body are shown in reference 6. Some data on aileron loads obtained on the present wing-body combination are presented in reference 7.

Data have been obtained at Mach numbers from 0.80 to 1.03, at angles of attack up to about 27°, and at aileron deflections between approximately ±15°. The test Reynolds number was about 7.0×10^6.

SYMBOLS

b_a	aileron span
c	wing local chord
c'	wing mean aerodynamic chord
c_a	aileron chord at any spanwise station
$\bar{c}_a$	aileron average chord

$C_{h,a}$ aileron hinge-moment coefficient, $\frac{\text{Hinge moment about hinge line}}{2qM'}$

$c_{n,a}$ aileron section normal-force coefficient, $\int_0^{1.0} \left(C_{p,l} - C_{p,u}\right) d\left(\frac{x}{c_a}\right)$

$C_{N,a}$ aileron normal-force coefficient, $\frac{\text{Aileron normal force}}{qS_a}$

$C_{h_\alpha} = \left(\frac{\partial C_h}{\partial \alpha}\right)_\delta$

$C_{h_\delta} = \left(\frac{\partial C_h}{\partial \delta}\right)_\alpha$

M free-stream Mach number

M' area moment of aileron about aileron hinge axis

C_p pressure coefficient, $\frac{p_{local} - p}{q}$

p free-stream static pressure

q free-stream dynamic pressure

S_a aileron area

x chordwise distance from aileron hinge line

x_{cp} distance from aileron hinge line to aileron center of pressure measured in aileron chord plane and parallel to model plane of symmetry (positive to rear of hinge line)

y lateral distance from inboard edge of aileron

y_{cp} lateral distance to aileron center of pressure measured from inboard edge of aileron (positive outboard)

α angle of attack of model (body reference line)

δ aileron deflection angle relative to wing-chord plane, measured in plane perpendicular to aileron hinge axis (considered positive when trailing edge is down on either wing)

δ_n nominal aileron deflection (not corrected for deflection due to load)

Λ sweep angle

Subscripts:

l aileron lower surface

u aileron upper surface

Subscripts outside the parentheses denote parameters maintained constant.

MODEL AND APPARATUS

Model and Instrumentation

The wing had a 45° sweep of the quarter-chord line and was mounted in a midwing position on the body at zero incidence. The wing airfoil sections (streamwise) were NACA 65A004, and the wing was designed with no geometric twist or dihedral. The fuselage was a cylindrical body of revolution with an ogival nose and a slightly boattailed afterbody. Pertinent dimensions and geometric details of the model are given in figure 1, and photographs of the model are shown as figure 2. Coordinates of the wing are given in reference 4, and the fuselage ordinates are given in reference 6.

The unbalanced trailing-edge ailerons were composed of four segments and were deflected in adjacent pairs to simulate inboard, midspan, and outboard ailerons. Tongues were mounted between the ailerons and the wing at the hinge line in order to permit various aileron deflection angles. These tongues were bent in order to obtain nominal deflections of 0°, ±7.5°, and ±15°, measured perpendicular to the hinge line. On the right wing the tongue for each segment covered most of the span in the gap between the wing and the aileron at the hinge line. The right inboard aileron was instrumented with four chordwise rows of static-pressure orifices arranged as shown in a table given in figure 3(a).

On the left wing two separate tongues, 0.86 inch wide spanwise, were utilized to attach each of the four segments. A gap of about

0.4 percent of the wing chord, therefore, existed over 71 percent of the aileron span. Strain-gage balances were mounted on each of the tongues to measure the aileron normal forces and hinge moments (fig. 3(b)).

Tunnel and Model Support

The tests were conducted in the Langley 16-foot transonic tunnel, which is an atmospheric wind tunnel with an octagonal, slotted test section permitting a continuous variation in speed to Mach numbers slightly above 1.0. The sting-support system is arranged so that the model is located near the center of the tunnel at all angles of attack.

TESTS

Measurements of aileron hinge moments and normal forces by use of strain-gage balances on the left wing were obtained at the conditions given in table I.

Pressures were measured on the right-wing inboard aileron at nominal deflection angles, δ_n, of 0°, $\pm 7.5^\circ$, and $\pm 15^\circ$. The angle of attack was varied from about 0° to about 21° at Mach numbers of 0.80, 0.90, 0.94, 0.98, and 1.03.

The Reynolds number, based on wing mean aerodynamic chord, varied from about 6.7×10^6 to 7.7×10^6.

ACCURACY

The measurement of Mach number in the test region is believed to be accurate within ±0.005, and the angles of attack presented are estimated to be correct within $\pm 0.1^\circ$.

The deflection angles of the aileron were determined from the nominal deflection and the deflection due to load. This deflection due to load was obtained from a static loading calibration. The values of δ presented are believed to be correct within $\pm 0.25^\circ$.

Effects of wing flexibility on the stain-gage measurements were accounted for by static loading calibrations of the wing. Elastic properties of the wing with no ailerons obtained from static loadings are given in reference 6.

RESULTS

Most of the results are presented for three representative Mach numbers only ($M = 0.80$, $M = 0.94$, and $M = 1.03$). The loading characteristics of the aileron are illustrated in the following figures:

	Figures
Inboard-aileron chordwise pressure distributions	4 to 6
Spanwise loading over inboard aileron	7
Comparisons of pressure and force measurements	8 and 9
Aileron hinge-moment characteristics	10 and 12
Aileron normal-force characteristics	11 and 13
Effect of Mach number on hinge-moment parameters	14
Aileron center-of-pressure locations	15 to 18

DISCUSSION

Pressure-Distribution Measurements

Chordwise pressure-distribution measurements obtained over the right inboard aileron are presented in figures 4, 5, and 6 for Mach numbers of 0.80, 0.94, and 1.03, respectively. Chordwise plots are shown for four spanwise positions on the aileron at nominal deflections of $\pm 15^\circ$, $\pm 7.5^\circ$, and 0°, and at angles of attack from 0° to 20° in increments of 4°.

The pressure distributions for subsonic speeds (fig. 4) show that with the control undeflected, the aileron chordwise loading was generally triangular in shape up to angles of attack of about 12°, but at angles of attack larger than this value the outboard sections started to stall, as was also noted with the loading on the wing in reference 6. With increasing positive or negative control deflection at moderate angles of attack, the loading tended to assume a more inward curved triangular shape with peak suction pressures occurring at the hinge line. Above $\alpha = 12^\circ$, the loading shape became irregular and upper-surface separation occurred at about $\alpha = 20^\circ$.

At a Mach number of 0.94, there was considerable variation in the loading shapes with spanwise position at all control deflections and at most angles of attack (fig. 5). At $M = 0.94$ the high suction peaks at the hinge line generally decreased from the values observed at a Mach number of 0.80. The section where $y/b_a = 0.978$ shows the effect of the flow-field shock (ref. 6) on the loading at positive aileron deflections (for example, see fig. 5(b)).

The load shapes at $M = 1.03$ (fig. 6) generally resembled those at $M = 0.94$ but usually showed both increased loading near the trailing edge at the lower angles of attack and less tendency for upper-surface separation at the highest angles of attack. The predominant characteristic of the loading for this aileron at transonic speeds was the irregular shapes which are not amenable to prediction methods in this speed range (ref. 8).

The variation of loading parameter over the span of the inboard aileron is presented in figure 7 for three Mach numbers at increments of about 4° in angle of attack. Data are shown for the five deflection angles investigated. The loading shape changed in the spanwise direction because of end effects at the outboard edge and of the interference of the body at the inboard section. This change was most apparent at $\delta = -15^\circ$ at the highest angles of attack, where the aileron load approached zero at the inboard station. Generally, changes in angle of attack had a larger effect on the shape of the spanwise loading curves than did changes in Mach number. At Mach numbers of 0.80 and 0.94 the aileron spanwise loading shapes were generally similar up to an angle of attack of 20°; however, above an angle of attack of 12° a disturbance originating on the wing at the juncture of the wing leading edge and the fuselage (ref. 6) passed over the outer portion of the aileron and altered the spanwise loading shape over the control. This disturbance caused the loading parameter at the station where $y/b_a = 0.543$ to become more positive at the higher angles of attack. At a Mach number of 1.03 this positive load-parameter increase at the station where $y/b_a = 0.543$ was delayed to the highest angles of attack.

Comparison of Pressure and Force Data

Typical comparisons of the hinge-moment and normal-force coefficients of the inboard aileron, obtained from strain-gage-balance measurements on the left wing and integrated pressure measurements on the right wing, are given in figures 8 and 9. Deviations in both the hinge-moment and normal-force results obtained from the two techniques generally occur at the same conditions. Some differences in deflection angles exist between the left- and right-wing ailerons because of different

stiffnesses of the wing attachment tongues. Despite these differences, the agreement of the two types of measurements is good.

The hinge-moment data of figure 8 and the normal-force data of figure 9 both show regular variations with angle of attack in the range between $\alpha = 0^\circ$ and $\alpha = 8^\circ$. In the region between $\alpha = 8^\circ$ and $\alpha = 12^\circ$, slope discontinuities occurred which were greatest at a Mach number of 0.94 and were probably caused by the shock originating at the wing-leading-edge—fuselage juncture sweeping back over the outboard region of the aileron (ref. 6). This effect can be seen in figure 5(d) where the load at the outboard station has been reduced from that at $\alpha = 8^\circ$ (fig. 5(c)) and in the spanwise loading distributions of figure 7(b). At angles of attack larger than 12° the sweep angle of the juncture shock changed very little, and the effect of the shock was felt over about the same area of the aileron but was obscured by the wing separation which had progressively crept inboard on the wing. The slopes of the hinge-moment and normal-force curves are, therefore, again generally regular at all Mach numbers up to the highest angles of attack.

Strain-Gage Measurements

The basic hinge-moment data such as shown in figure 8 have been cross-plotted in order to obtain values of the hinge-moment characteristics of the ailerons at constant values of angle of attack as shown in figure 10. Generally, the variation of hinge-moment coefficient with aileron-deflection angle became more nonlinear as the angle of attack was increased. At the higher angles of attack, however, the hinge-moment variation with deflection for the inboard and midspan ailerons became more nearly linear as the Mach number was increased because of the flow becoming supersonic over greater portions of the aileron.

The outboard aileron was subjected to the first occurrences of wing-tip stall and the sweeping back of the juncture shock from the leading edge of the wing; therefore, this control showed the nonlinearities due to model attitude at lower angles of attack than did the more inboard controls. At an angle of attack of about 8°, the slope of the hinge-moment curve for the outboard aileron reversed at positive deflections. A similar reversal of hinge-moment slope was also observed with the swept-wing aileron of reference 2 at Mach numbers of 0.95 and 1.00. Some tendency toward reduced rolling effectiveness at positive aileron deflections was also noted for the outboard aileron of the present wing in the results of reference 5. It is believed that this tendency was primarily the result of separation at the swept-wing tip combined with some reduction in wing-tip angle of attack caused by aerodynamic twist (ref. 6); both results tend to reduce aileron load and negative hinge moments. The chordwise center-of-pressure locations of figure 15

also indicate that the center of pressure moves forward with increasing aileron deflection at high angles of attack.

Strain-gage measurements of the variation of aileron normal-force coefficient with deflection are shown in figure 11. Some of the conditions shown on the hinge-moment results of figure 10 were not included in the aileron normal-force data because of malfunctions of the data recording system. The data for the outboard aileron (fig. 11(c)) at a Mach number of 0.90 are indicated by broken lines, since only the data for deflections of 7.5° and -7.5° were available. The slopes of the normal-force curves generally decreased somewhat at the higher angles of attack. Aileron stall was indicated in the positive deflection region because of the cumulative effects of angle of attack and control deflection.

The hinge-moment and normal-force data obtained from pressure measurements on the inboard aileron (figs. 12 and 13) are generally similar to the corresponding data obtained with strain gages. The pressure data, however, show less tendency for the slope of the curve of the normal-force coefficient to decrease at high positive aileron deflections than does the strain-gage measurements.

The variations of the hinge-moment parameters, C_{h_δ} and C_{h_α}, with Mach number are presented in figure 14 to illustrate the effect of aileron spanwise position on these parameters. Slopes were obtained in the region near $\alpha = 0^\circ$ or $\delta_a = 0^\circ$, where the hinge-moment curves were generally linear, and are valid for only low angles of attack and small control deflections. No significant differences in C_{h_δ} exist between the three aileron locations. A gradual increase in C_{h_δ} occurred between Mach numbers of 0.90 and 0.98 because of the movement of the flow-field shock back over the ailerons in this region. Above a Mach number of 0.98, C_{h_δ} remained essentially constant because supersonic flow had been established over the controls. The value of C_{h_α} was greatest for the inboard aileron and least for the outboard aileron, except at the highest Mach numbers where the inboard aileron had the lowest value of C_{h_α}, and the midspan aileron showed the highest value.

Inspection of the curves of figures 15 and 16, which show the variation of aileron chordwise center-of-pressure position with aileron deflection, indicates that definite trends with regard to control deflection or angle of attack are difficult to observe. However, qualitatively, there was a general rearward movement of the chordwise center of pressure with increasing Mach number. As would be expected, the control

deflection at which the center of pressure moves off the aileron became more negative as the angle of attack was increased.

The data for spanwise center of load shown in figures 16 and 17 reveal no particular trends with angle of attack, control deflection, or Mach number for any of the three ailerons.

CONCLUSIONS

From the results of an investigation of the loading characteristics at transonic speeds of ailerons located at inboard, midspan, and outboard positions on a 45° sweptback-wing—body combination, the following observations are made:

1. The loading shapes over the flap-type controls with swept hinge lines are irregular and are difficult to predict from theoretical considerations in the transonic speed range.

2. The loading on the ailerons of this investigation was established by the flow characteristics of the basic sweptback wing with a shock originating from the juncture of the wing leading edge and the fuselage having the greatest effect on the loading.

3. No significant differences in the values of the slope of the curves of hinge-moment coefficient against aileron deflection for the three spanwise positions of the aileron were observed; generally the inboard aileron had the greatest value of the slope of the curves of hinge-moment coefficient against angle of attack and the outboard aileron had the least.

4. Changes in angle of attack generally had a larger effect on the shape of the inboard-aileron spanwise-loading curves than did changes in Mach number.

Langley Aeronautical Laboratory,
National Advisory Committee for Aeronautics,
Langley Field, Va., September 6, 1957.

REFERENCES

1. Thompson, Robert F.: Hinge-Moment, Lift, and Pitching-Moment Characteristics of a Flap-Type Control Surface Having Various Hinge-Line Locations on a 4-Percent-Thick 60° Delta-Wing - Transonic-Bump Method. NACA RM L54B08, 1954.

2. Thompson, Robert F.: Investigation of a 42.7° Sweptback Wing Model To Determine the Effects of Trailing-Edge Thickness on the Aileron Hinge-Moment and Flutter Characteristics at Transonic Speeds. NACA RM L50J06, 1950.

3. Hieser, Gerald: Transonic Investigation of the Effectiveness and Loading Characteristics of a Flap-Type Aileron With and Without Paddle Balances on an Unswept-Wing—Fuselage Model. NACA RM L56B02, 1956.

4. Critzos, Chris C.: A Transonic Investigation of the Static Longitudinal-Stability Characteristics of a 45° Sweptback Wing-Fuselage Combination With and Without Horizontal Tail. NACA RM L56A18, 1956.

5. Hieser, Gerald, and Whitcomb, Charles F.: Effectiveness at Transonic Speeds of Flap-Type Ailerons for Several Spanwise Locations on a 4-Percent-Thick Sweptback-Wing—Fuselage Model With and Without Tails. NACA RM L56J04, 1957.

6. Runckel, Jack F., and Lee, Edwin E., Jr.: Investigation at Transonic Speeds of the Loading Over a 45° Sweptback Wing Having an Aspect Ratio of 3, a Taper Ratio of 0.2, and NACA 65A004 Airfoil Sections. NACA RM L56F12, 1956.

7. Runckel, Jack F., and Gray, W. H.: An Investigation of Loads on Ailerons at Transonic Speeds. NACA RM L55E13, 1955.

8. West, F. E., Jr., and Czarnecki, K. R.: Loads Due to Controls at Transonic and Low Supersonic Speeds. NACA RM L57D26a, 1957.

TABLE I.- TEST CONDITIONS

Mach number, M	Nominal δ_n	Angle of attack, α, deg		
		Inboard aileron	Midspan aileron	Outboard aileron
0.80	-15°	0 to 25.0	-1.8 to 23.9	0 to 12.0
.90		0 to 25.2	-1.9 to 26.2	0 to 12.0
.94		0 to 21.4	-1.9 to 24.3	0 to 12.0
.98		0 to 21.5	-1.9 to 22.3	0 to 12.0
1.00		0 to 11.4	-1.9 to 13.7	0 to 12.0
1.03		-0.1 to 11.4	-1.9 to 13.7	0 to 12.0
0.80	-7.5°	0 to 24.9	-1.8 to 26.0	0 to 24.9
.90		0 to 25.2	-1.9 to 26.2	0 to 25.3
.94		0.3 to 25.4	-1.9 to 26.4	0 to 25.5
.98		0 to 25.4	-1.9 to 26.6	0 to 21.5
1.00		-0.3 to 12.3	-1.9 to 13.7	0 to 12.0
1.03		0.3 to 12.3	-1.9 to 13.7	0 to 12.0
0.80	0°	-3.5 to 23.9	-3.5 to 21.8	-3.5 to 23.9
.90		-3.6 to 26.2	11.5 to 26.2	11.4 to 26.2
.94		-1.4 to 26.4	-1.4 to 26.4	-1.4 to 26.4
.98		-3.6 to 26.5	-3.6 to 26.5	-3.6 to 26.5
1.00		-3.6 to 12.3	-3.6 to 12.3	-3.6 to 12.3
1.03		-3.6 to 10.5	-3.6 to 10.5	-3.6 to 10.5
0.80	7.5°	-0.1 to 24.9	-1.8 to 26.0	0 to 25.0
.90		-0.1 to 25.1	-1.9 to 26.2	0 to 25.3
.94		-0.1 to 19.4	-1.9 to 20.1	0 to 25.4
.98		-0.1 to 19.5	-1.9 to 20.2	0 to 21.6
1.00		-0.1 to 11.9	-1.9 to 11.6	0 to 12.0
1.03		-0.1 to 11.9	-1.9 to 11.6	0 to 12.0
0.80	15°	1.9 to 13.3	-1.8 to 15.6	
.90		0 to 11.9	-1.8 to 13.6	
.94		-0.1 to 11.9	-1.9 to 11.6	
.98		-0.1 to 11.9	-1.9 to 13.7	
1.00		-0.1 to 9.5	-1.9 to 13.5	
1.03		0 to 11.4	-1.9 to 13.7	

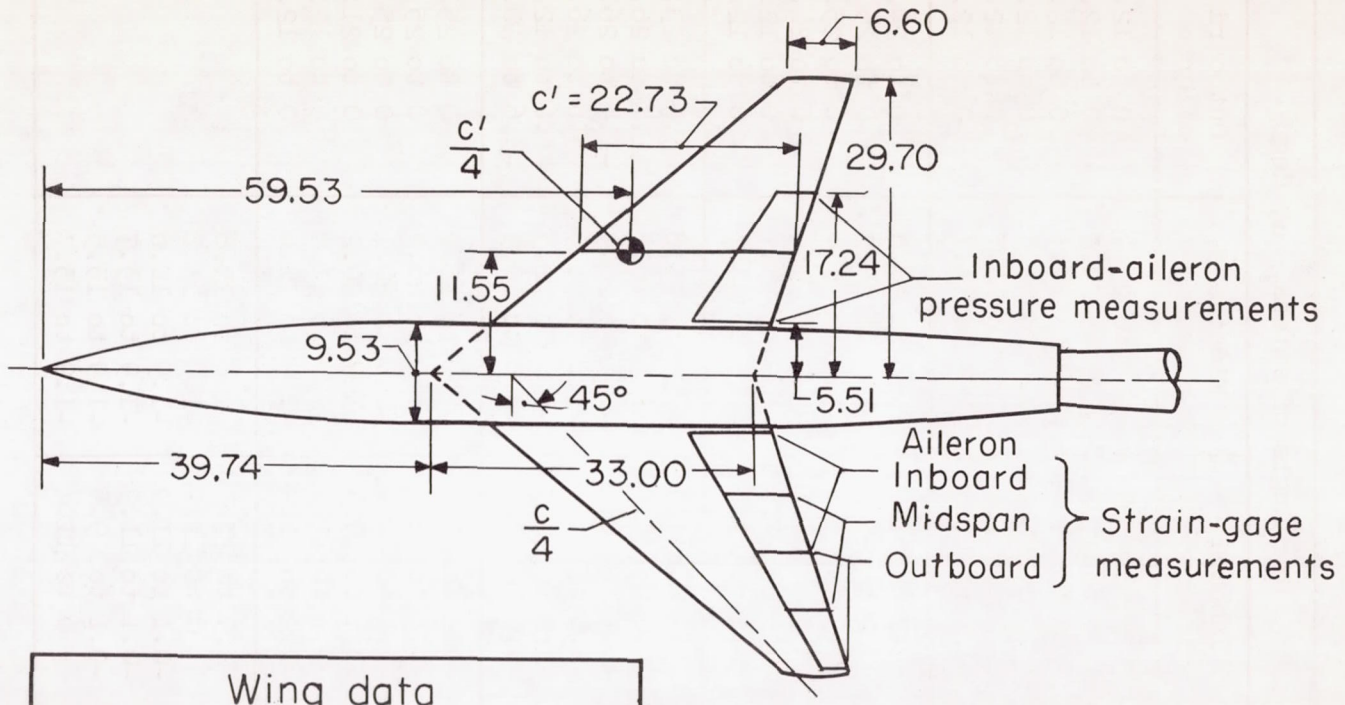

Wing data	
Aspect ratio	3.0
Taper ratio	0.2
Wing area	8.165 sq ft
Airfoil section	65A004

Figure 1.- Geometric details of model. All dimensions are in inches except as noted.

(a) Left-wing ailerons with strain gages. $\delta = 0^{\circ}$. L-57-2755

Figure 2.- Photographs of model ailerons.

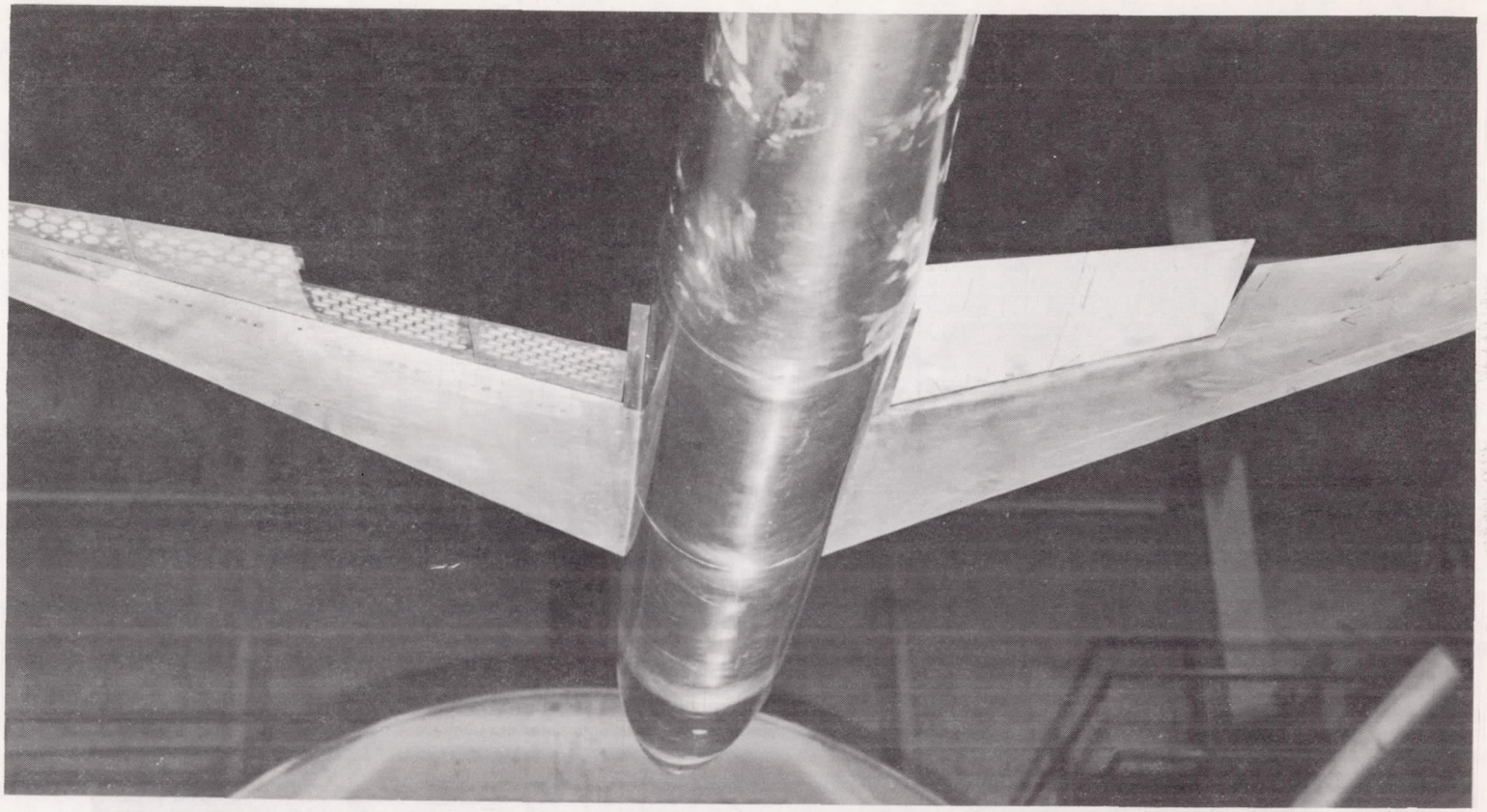

(b) Inboard ailerons of left and right wings deflected 15°. L-57-2756

Figure 2.- Concluded.

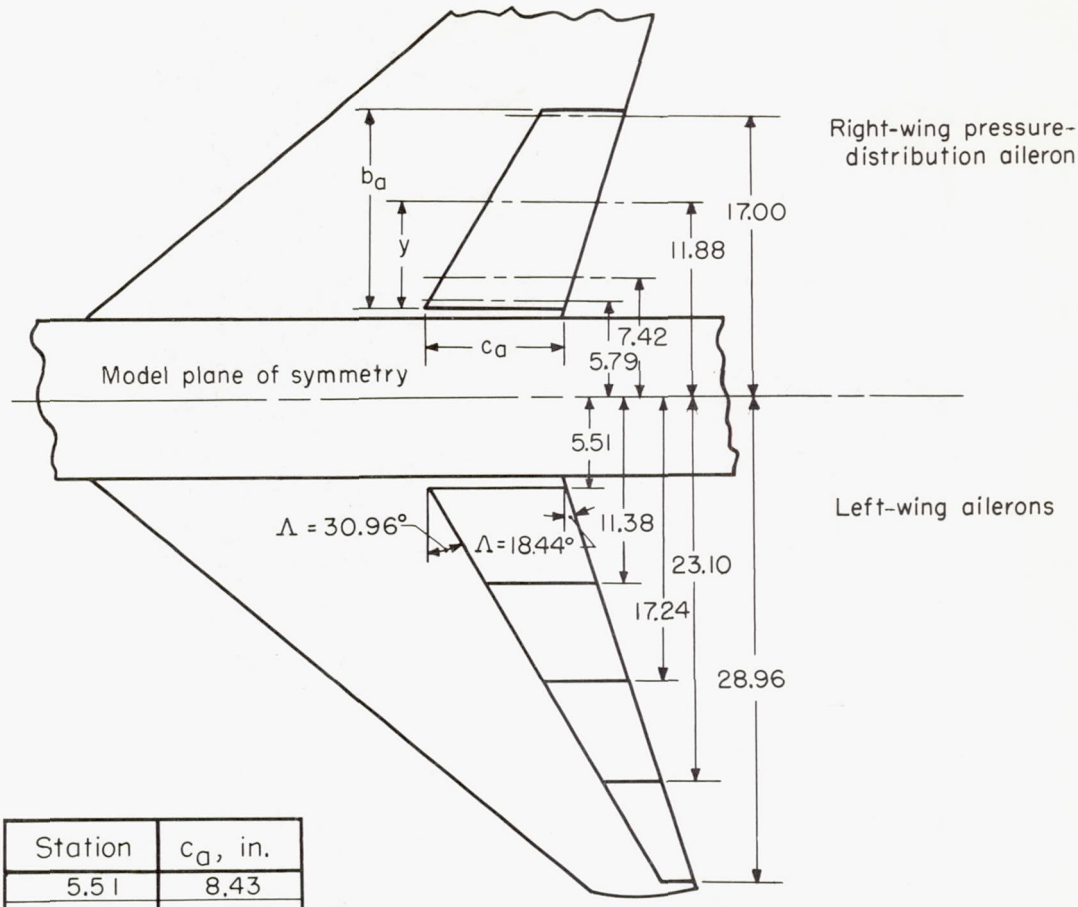

Station	c_a, in.
5.51	8.43
11.38	6.86
17.24	5.30
23.10	3.74
28.96	2.18

Aileron	b_a, in.	$\bar{c}_a$, in.	S_a, in.^{2}	M', in.^{3}
Inboard	11.68	6.88	80.21	240.23
Midspan	11.68	5.30	61.92	144.72
Outboard	11.68	3.74	43.67	73.92

Orifice Station	y/b_a	c_a	Pressure-Orifice Locations, x/c_a, Upper and Lower Surface
5.79	0.023	8.36	0, 0.167, 0.333, 0.500, 0.667, 0.833
7.42	.163	7.92	0, .167, .333, .500, .667, .833
11.88	.543	6.73	0, .167, .333, .500, .667, .833
17.00	.978	5.37	0, .167, .333, .500, .667, .833

(a) Dimensions and orifice locations.

Figure 3.- Aileron details.

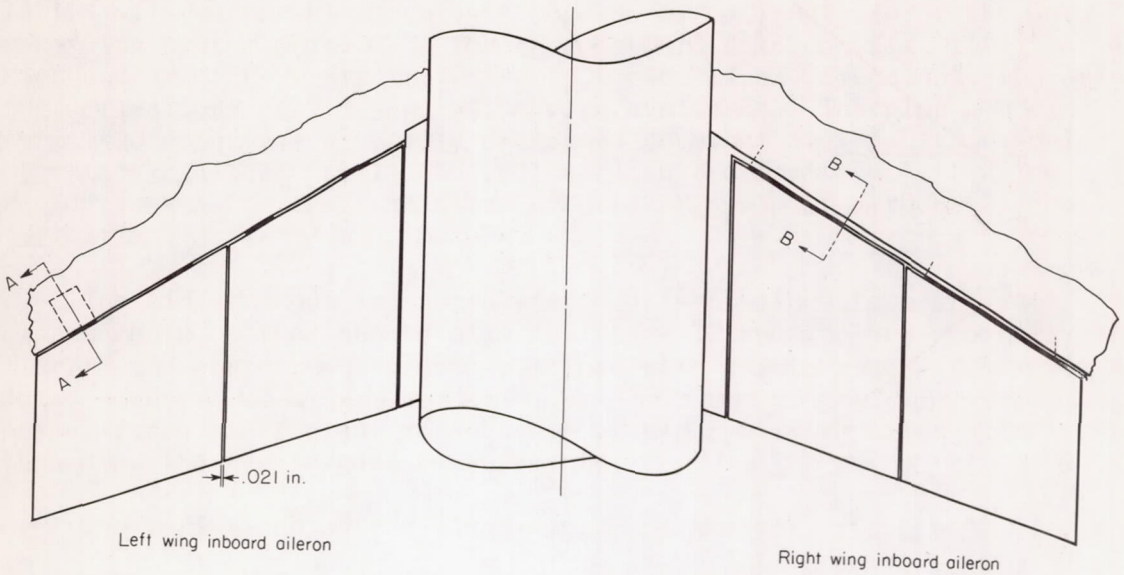

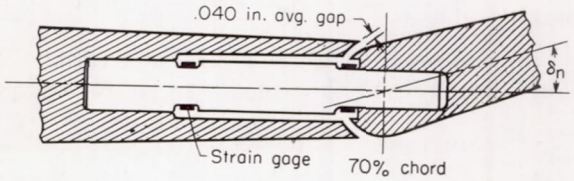

Section A–A

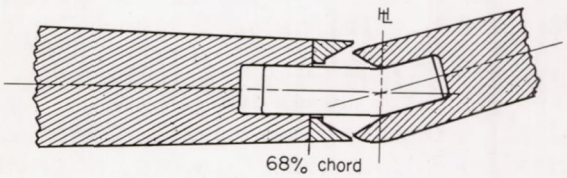

Section B–B

(b) Attachment details.

Figure 3.- Concluded.

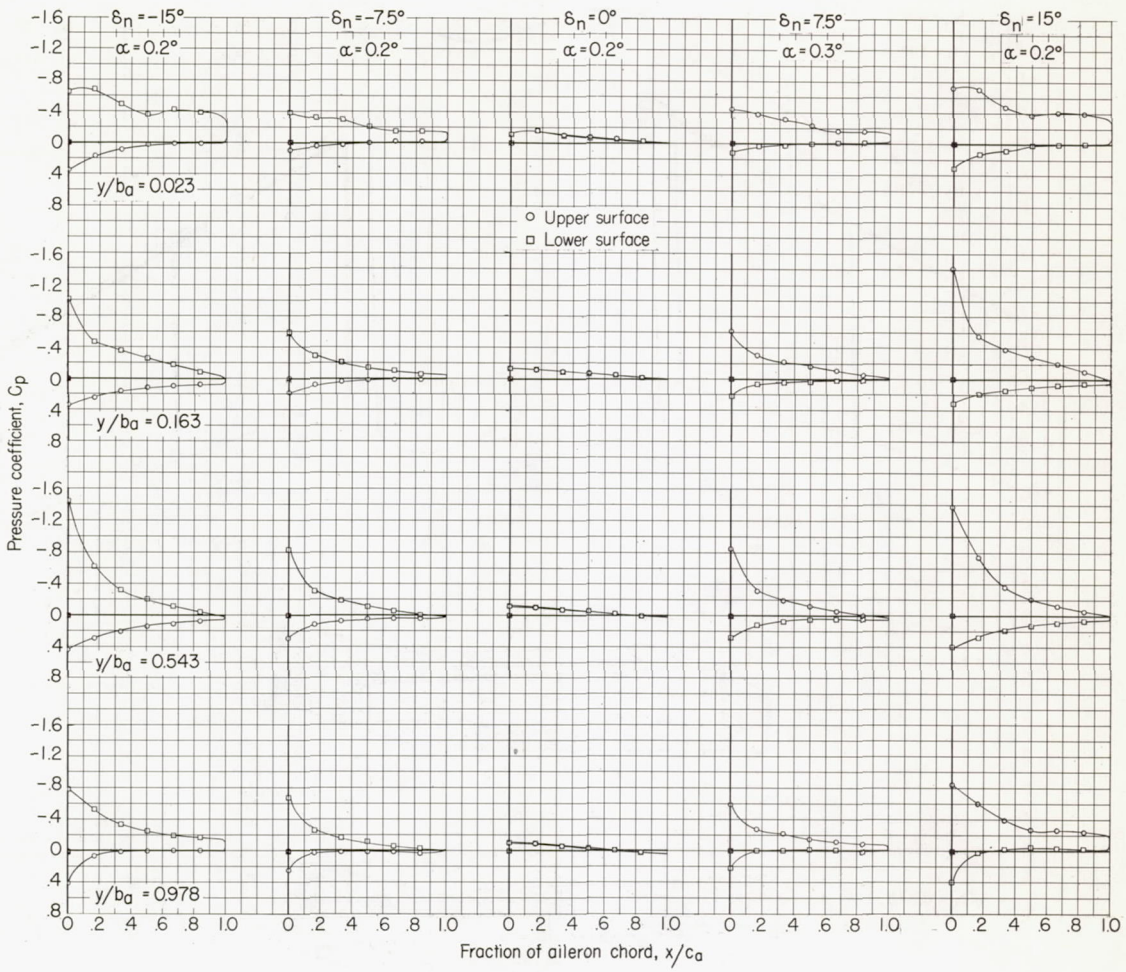

(a) $\alpha \approx 0^\circ$.

Figure 4.- Inboard-aileron chordwise pressure distributions. M = 0.80.

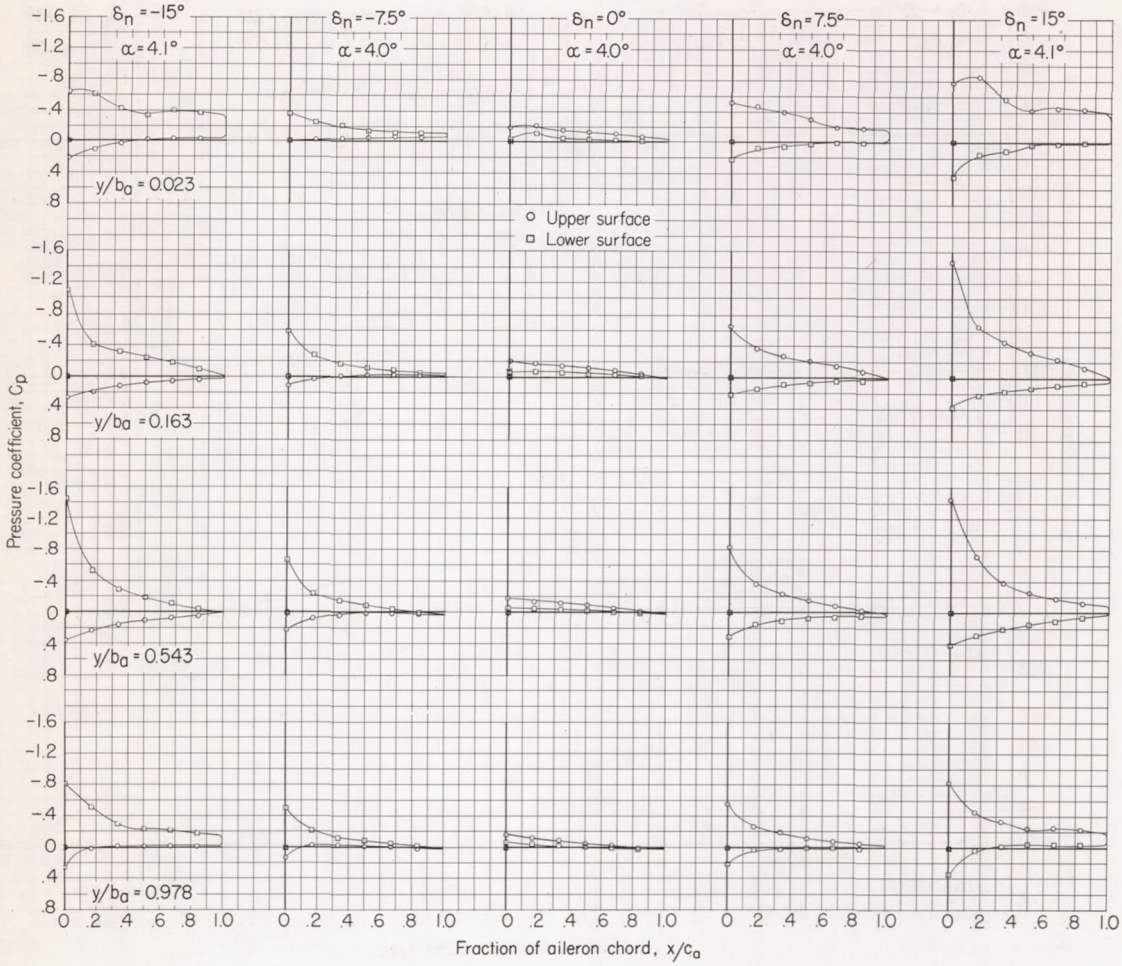

(b) $\alpha \approx 4°$.

Figure 4.- Continued.

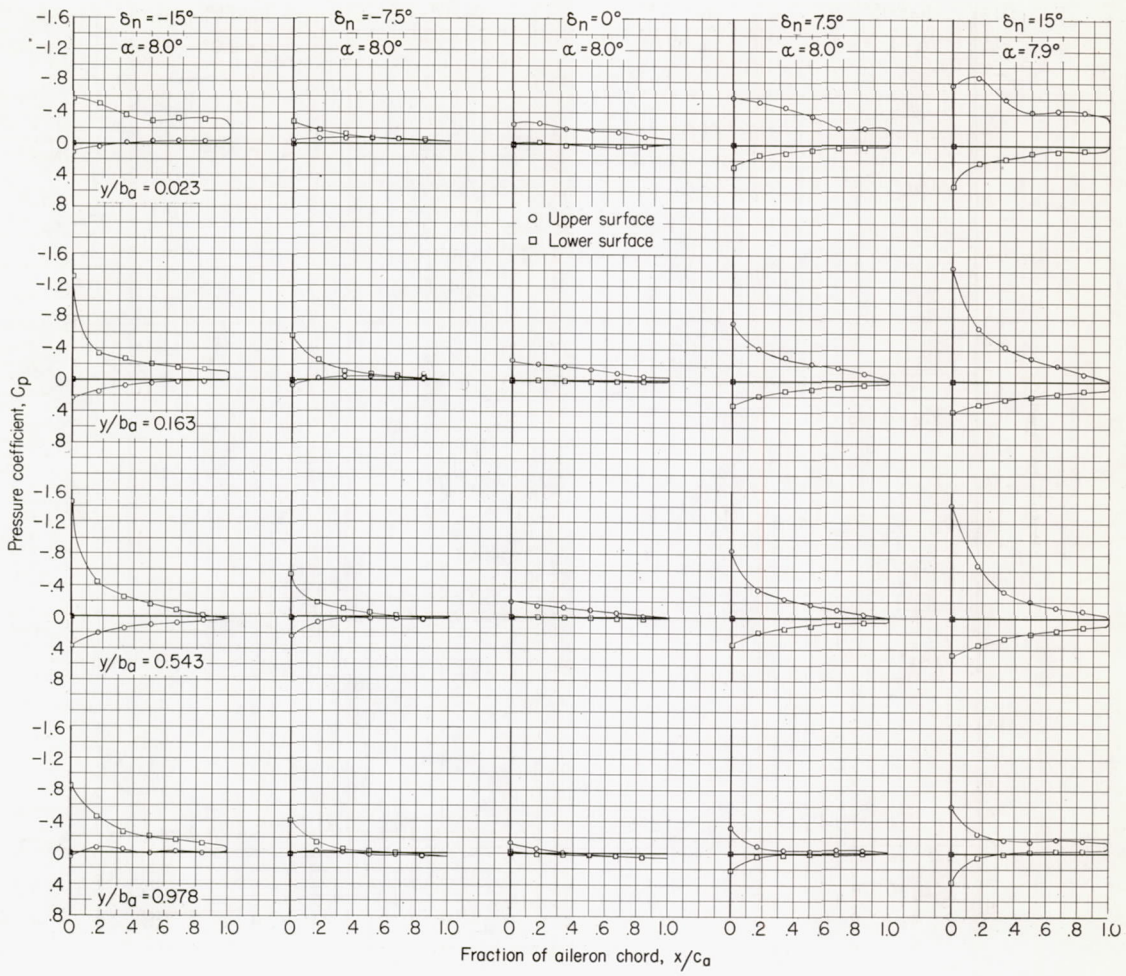

(c) $\alpha \approx 8°$.

Figure 4.- Continued.

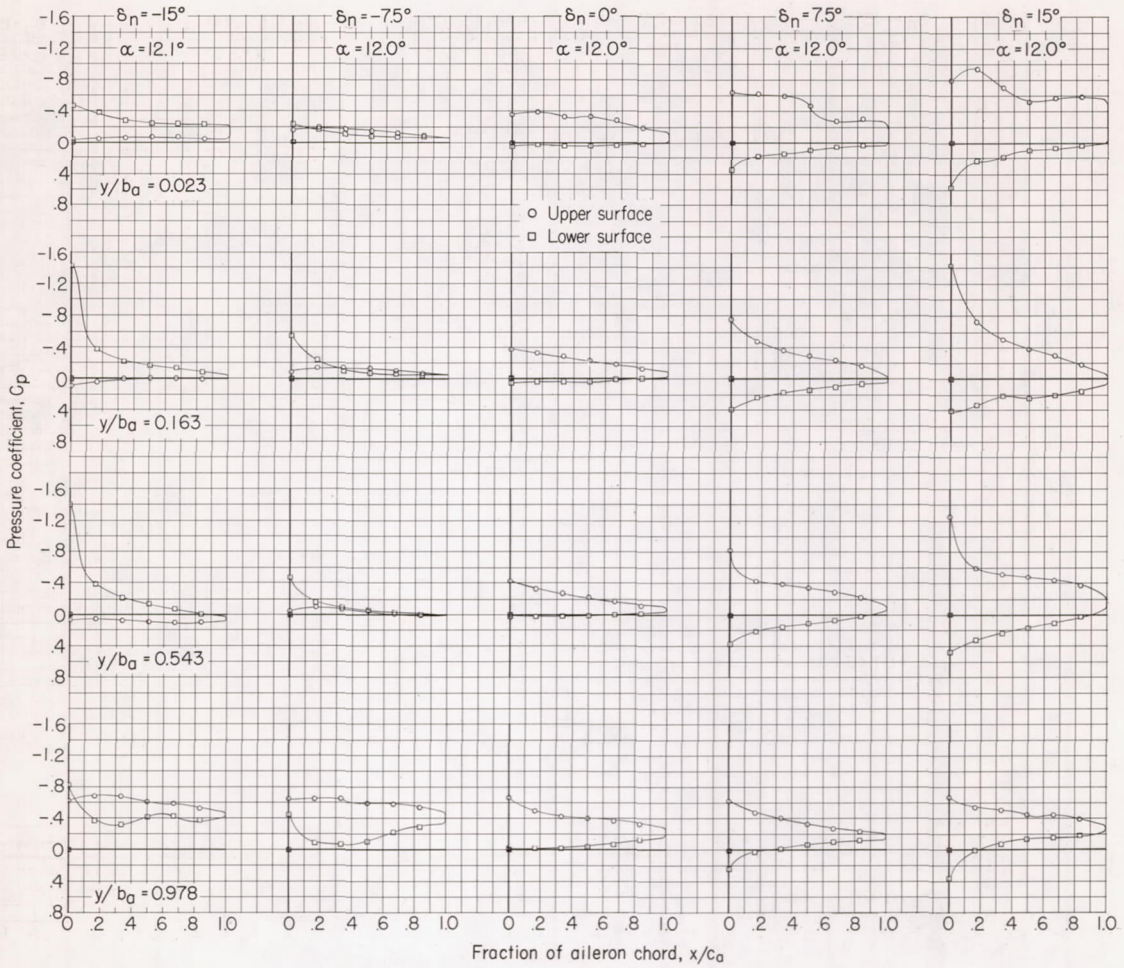

(d) $\alpha \approx 12°$.

Figure 4.- Continued.

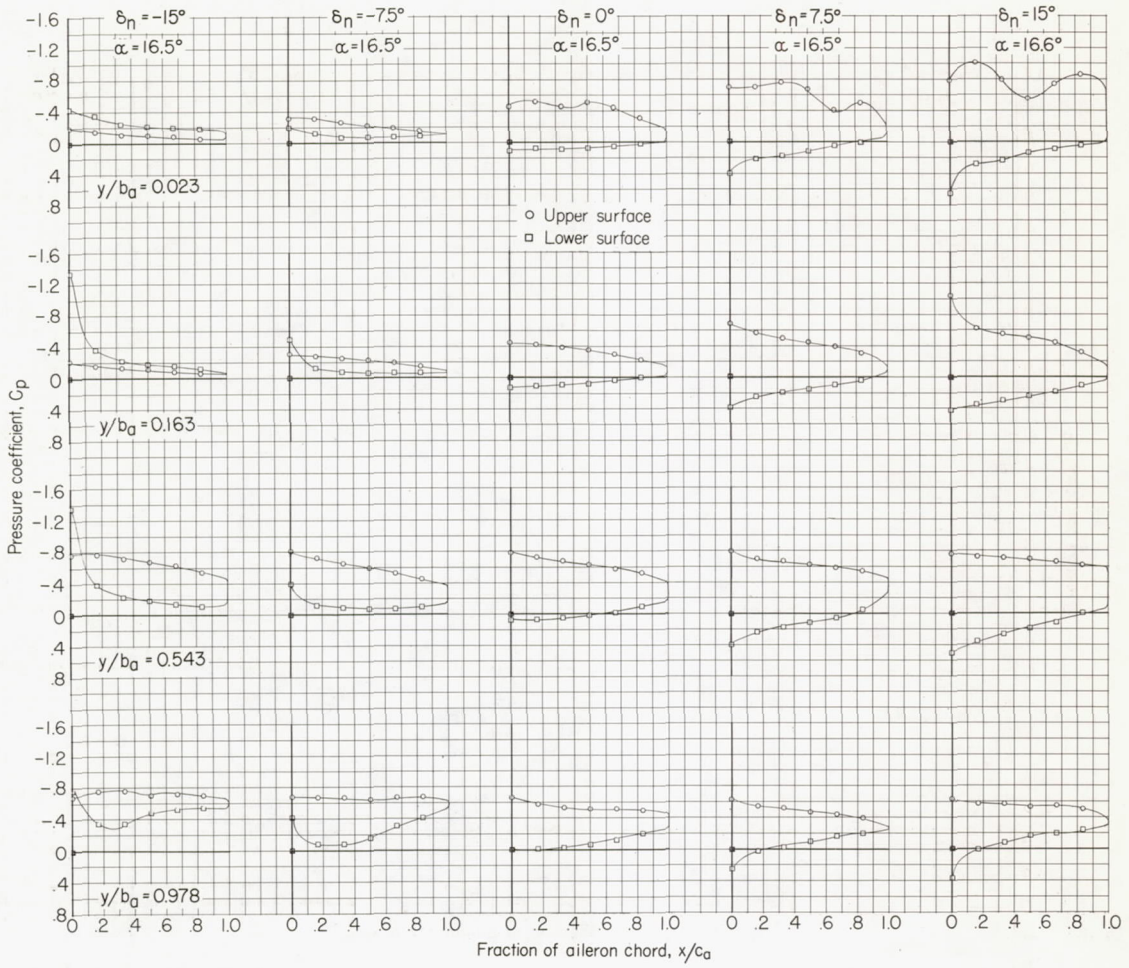

(e) $\alpha \approx 16.5^{\circ}$.

Figure 4.- Continued.

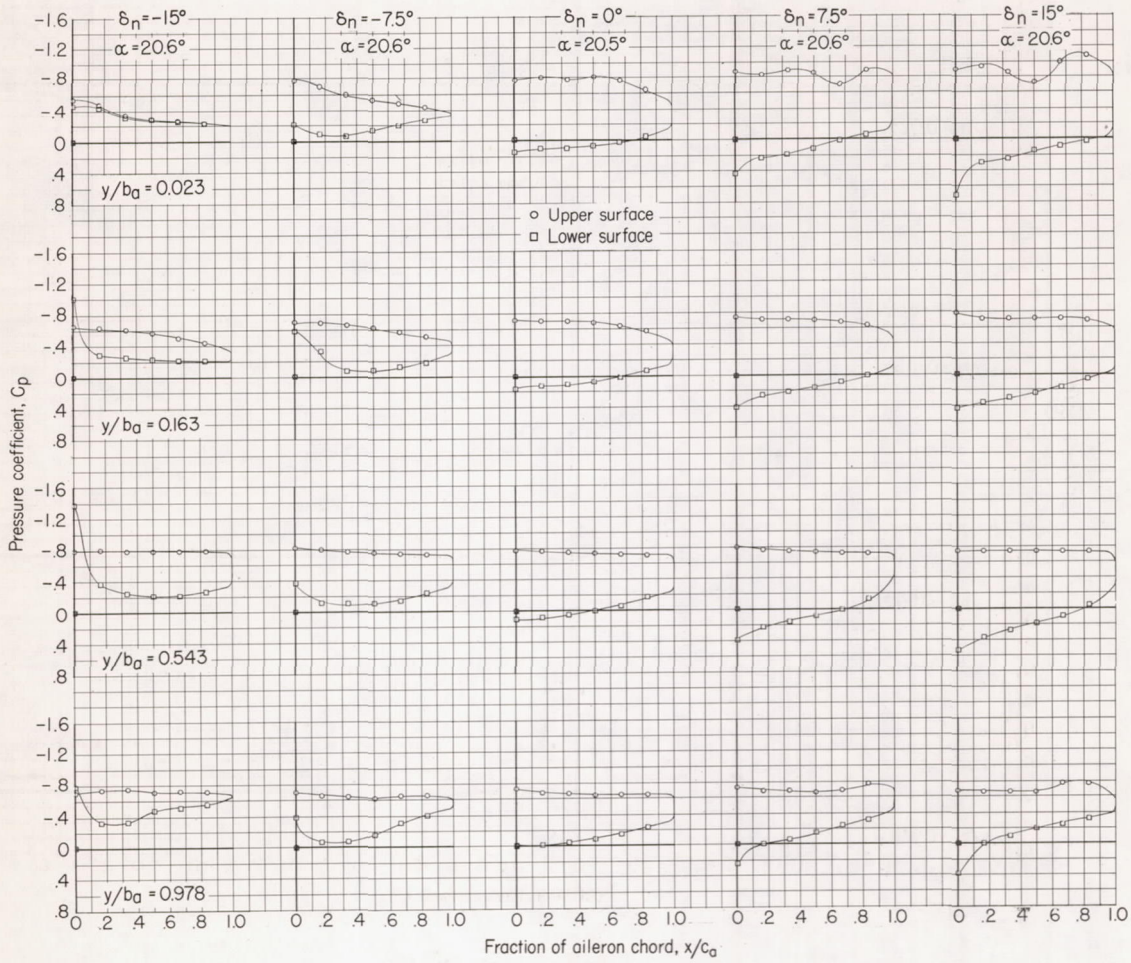

(f) $\alpha \approx 20.6^{\circ}$.

Figure 4.- Concluded.

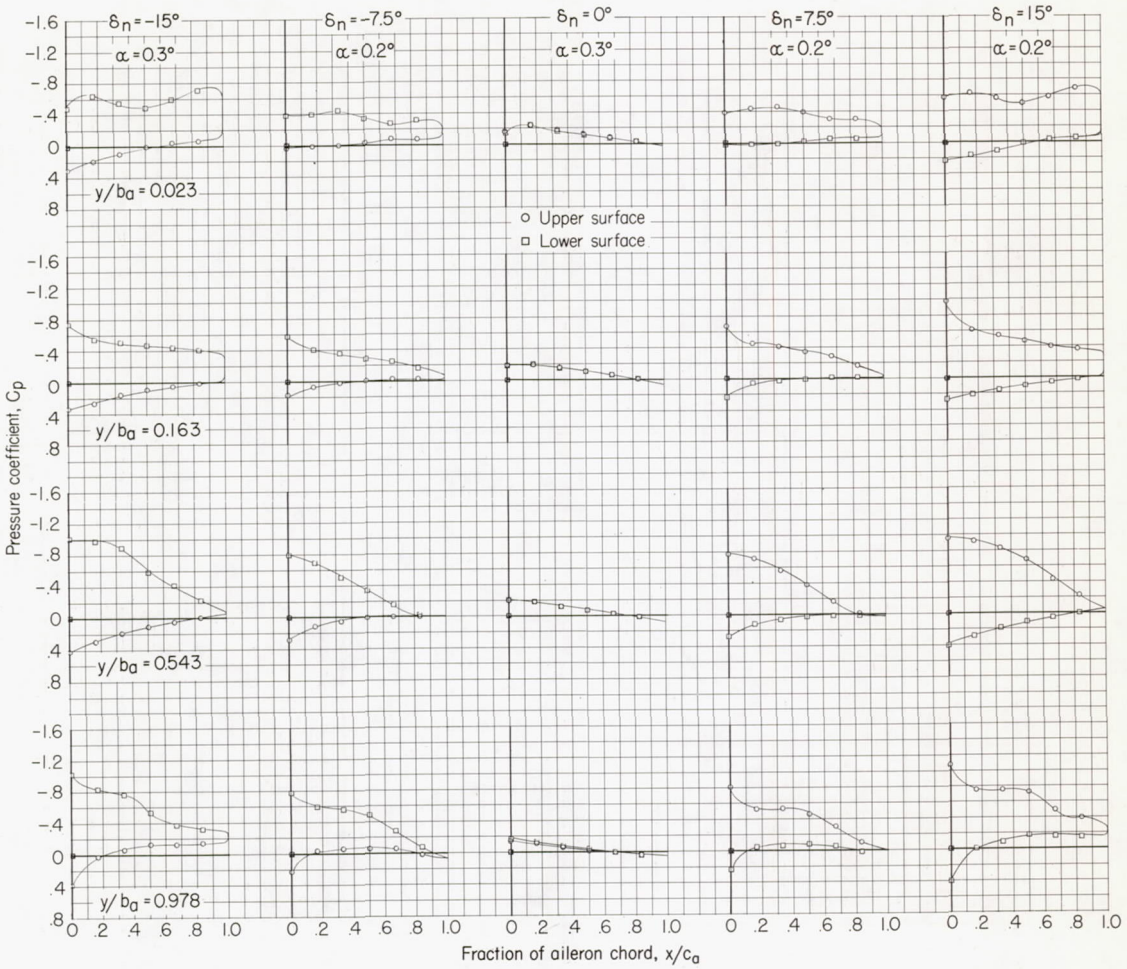

(a) $\alpha \approx 0.2^{\circ}$.

Figure 5.- Inboard-aileron chordwise pressure distribution. M = 0.94.

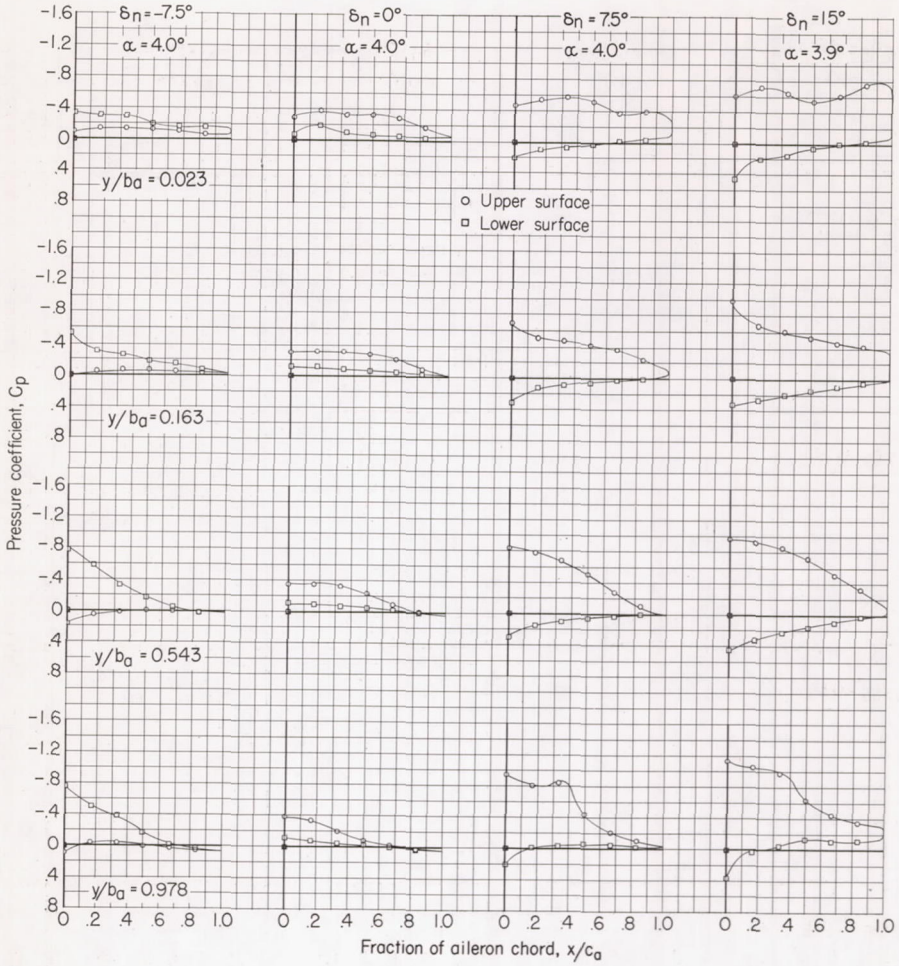

(b) $\alpha \approx 4^{\circ}$.

Figure 5.- Continued.

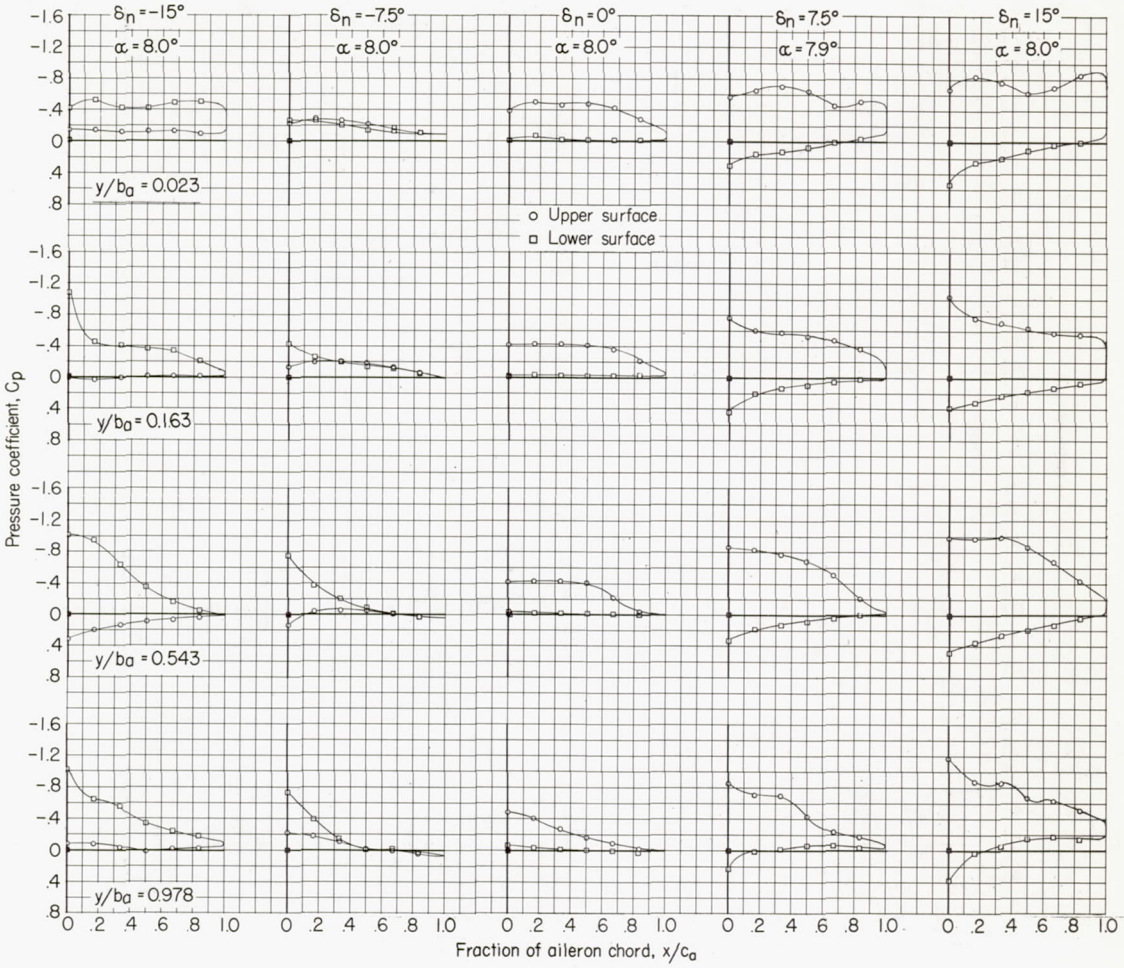

(c) $\alpha \approx 8^{\circ}$.

Figure 5.- Continued.

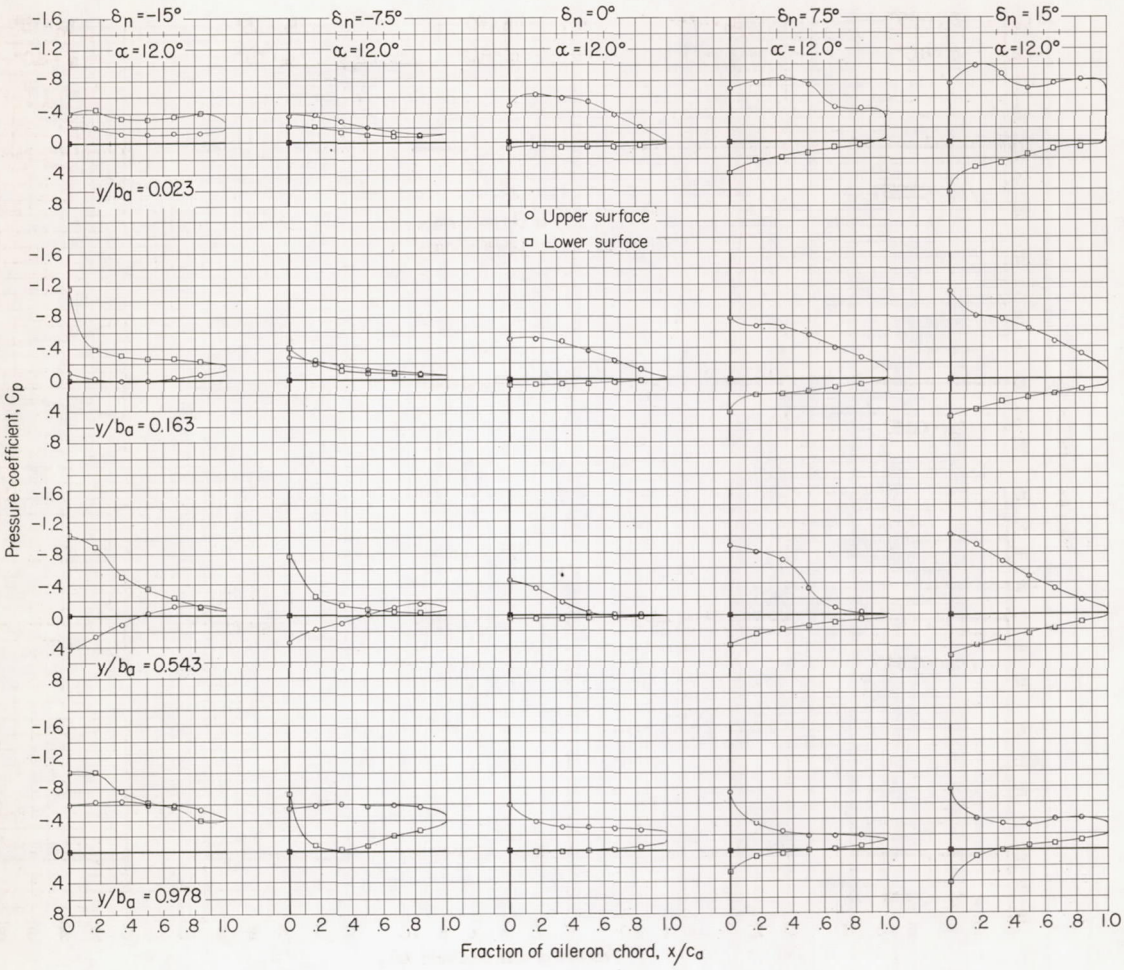

(d) $\alpha \approx 12^{\circ}$.

Figure 5.- Continued.

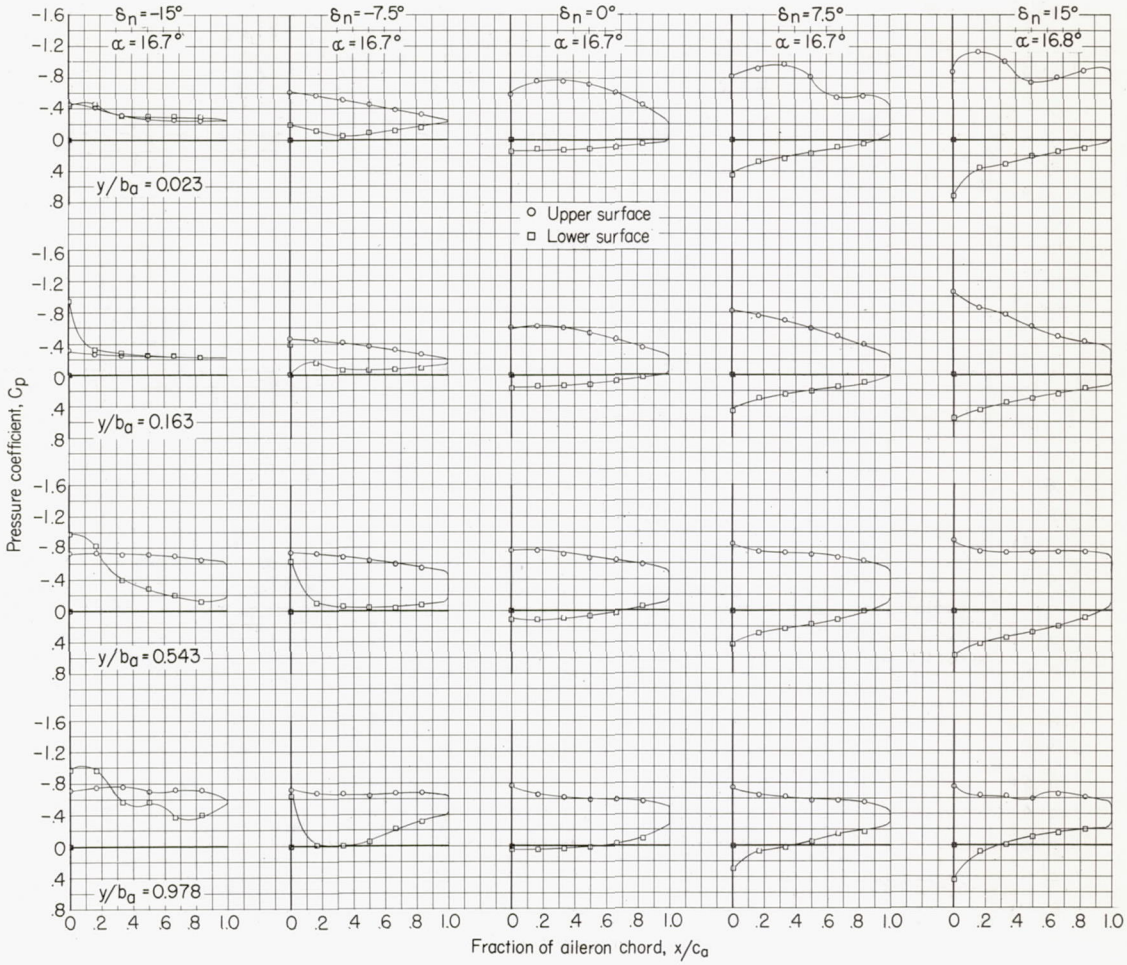

(e) $\alpha \approx 16.7^{\circ}$.

Figure 5.- Continued.

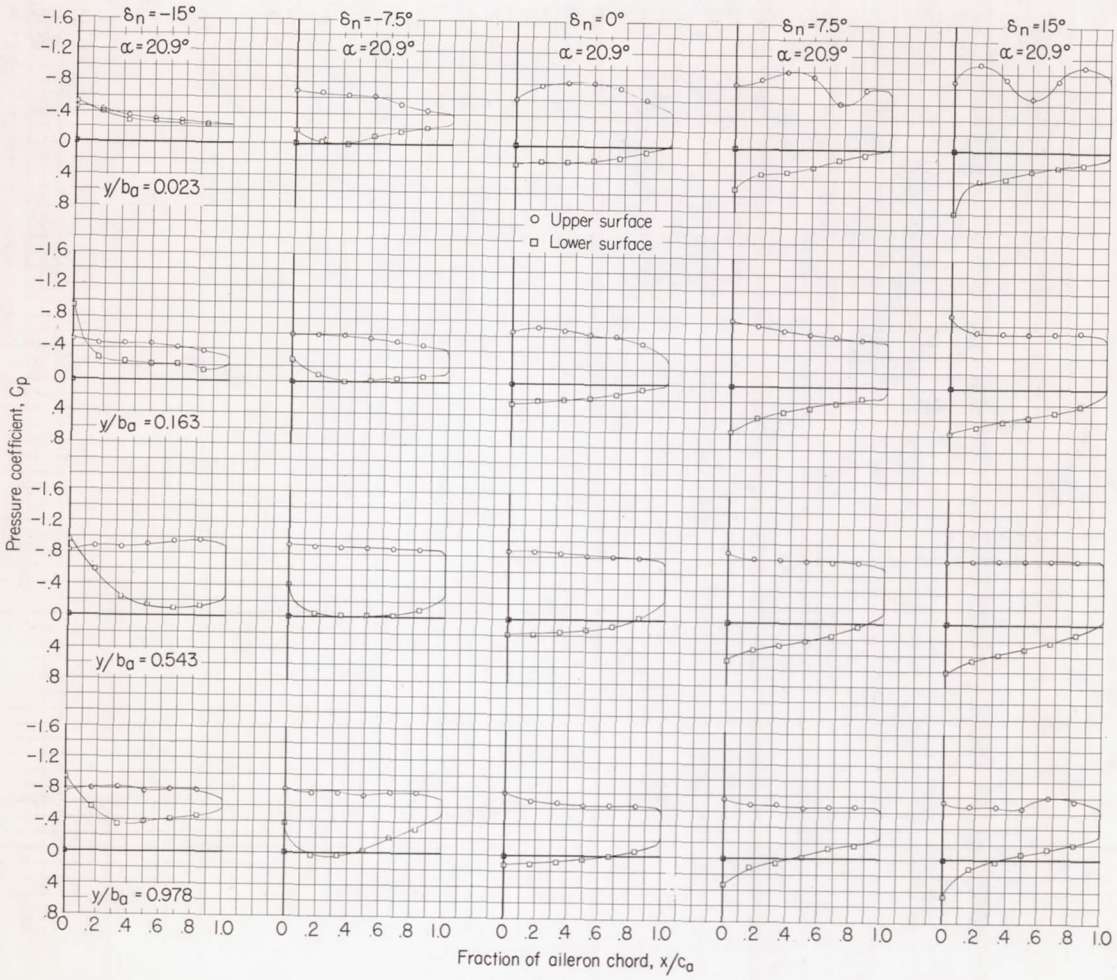

(f) $\alpha \approx 20.9°$.

Figure 5.- Concluded.

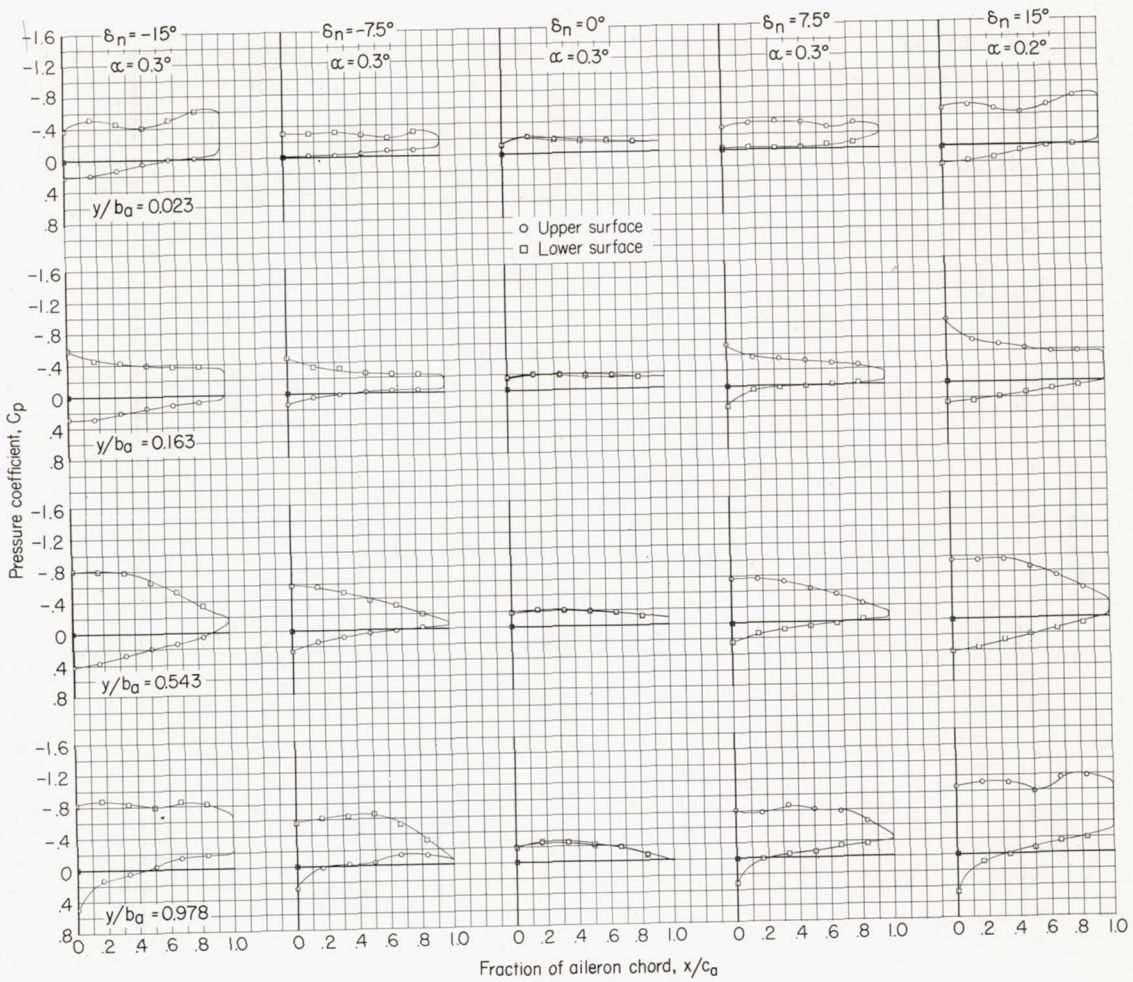

(a) $\alpha \approx 0.3^{\circ}$.

Figure 6.- Inboard-aileron chordwise pressure distribution. M = 1.03.

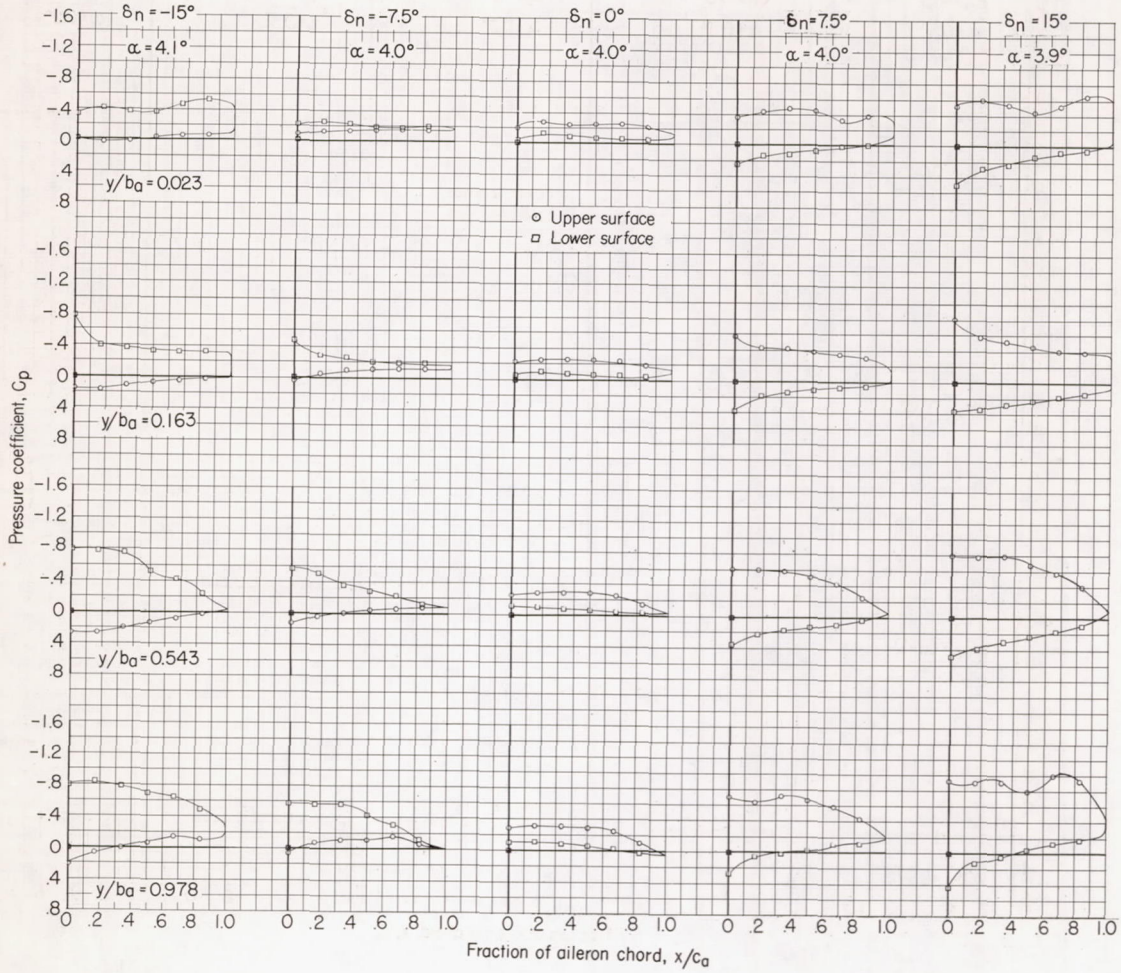

(b) $\alpha \approx 4^{\circ}$.

Figure 6.- Continued.

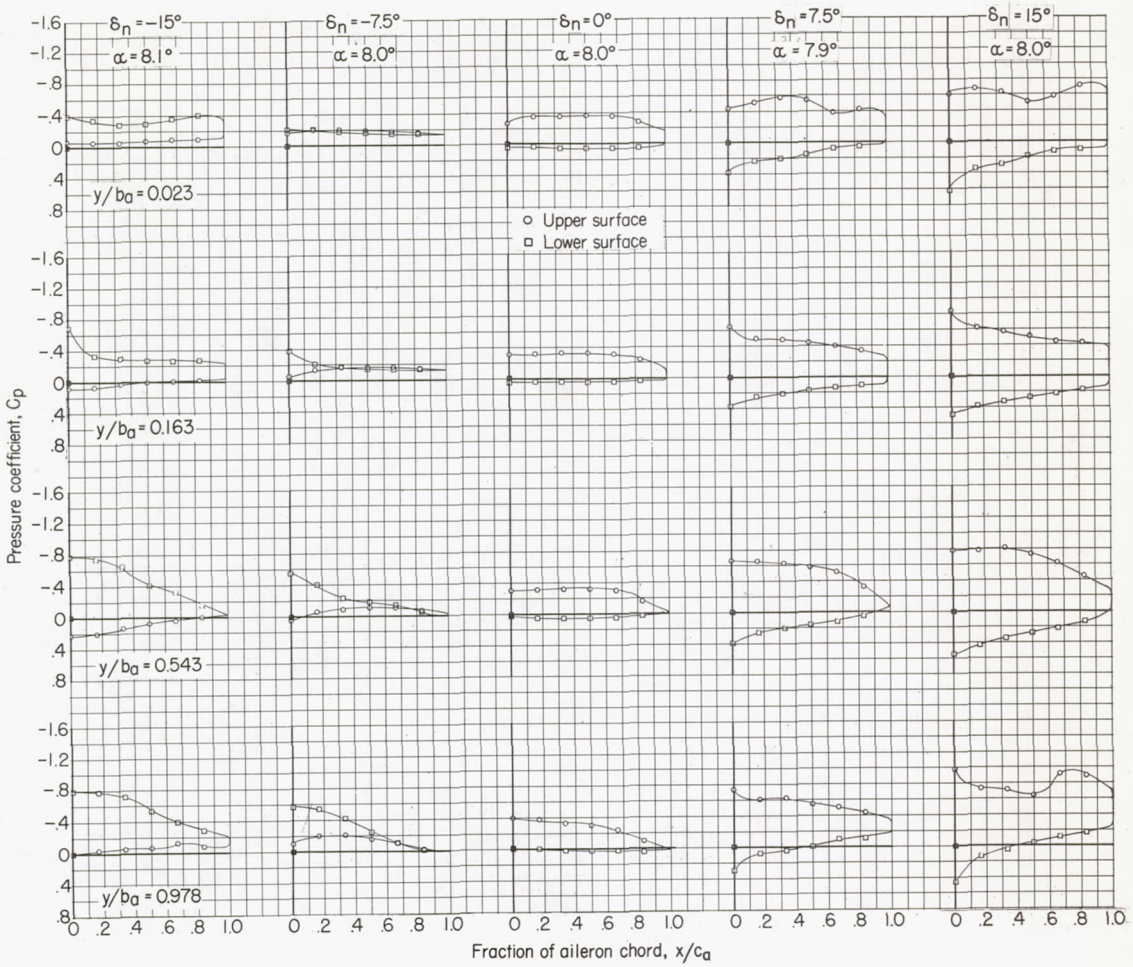

(c) $\alpha \approx 8°$.

Figure 6.- Continued.

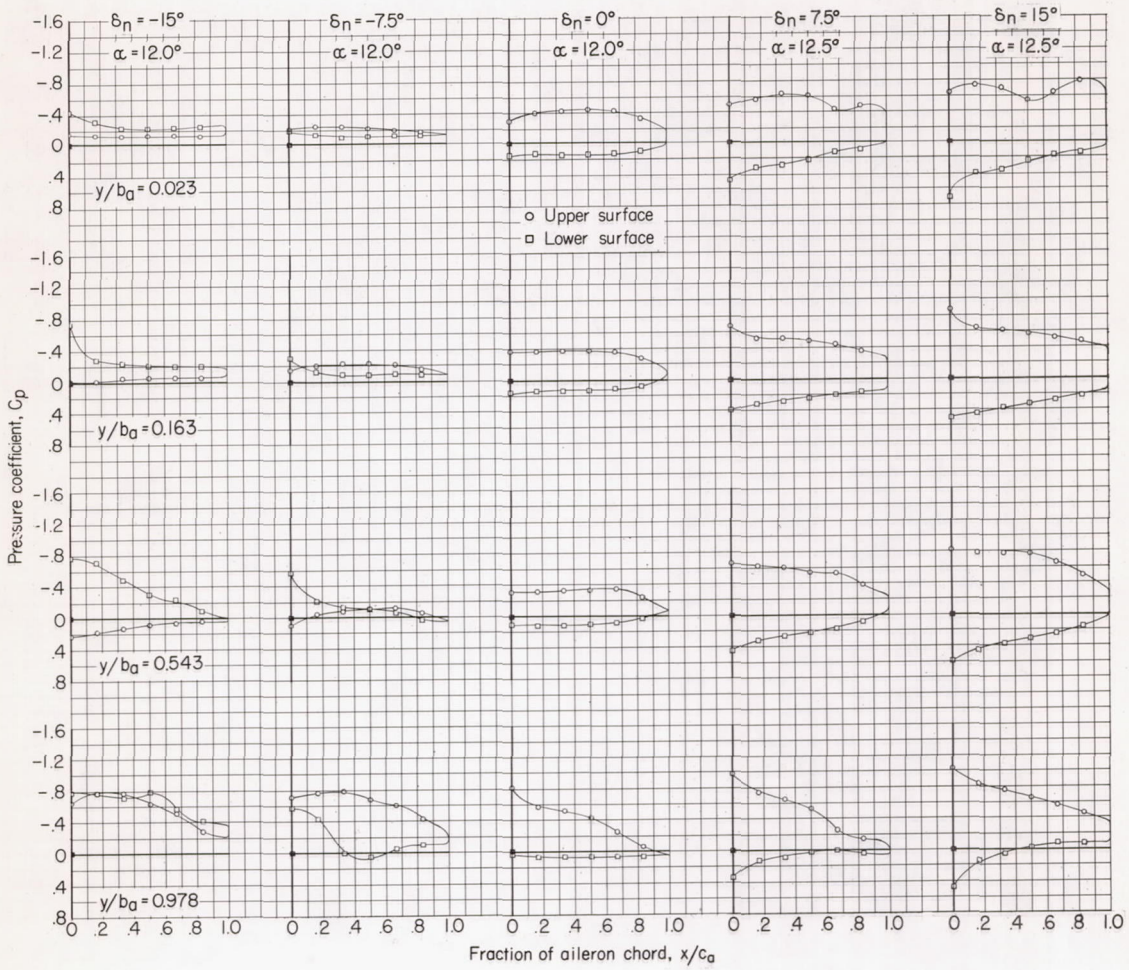

(d) $\alpha \approx 12^{\circ}$.

Figure 6.- Continued.

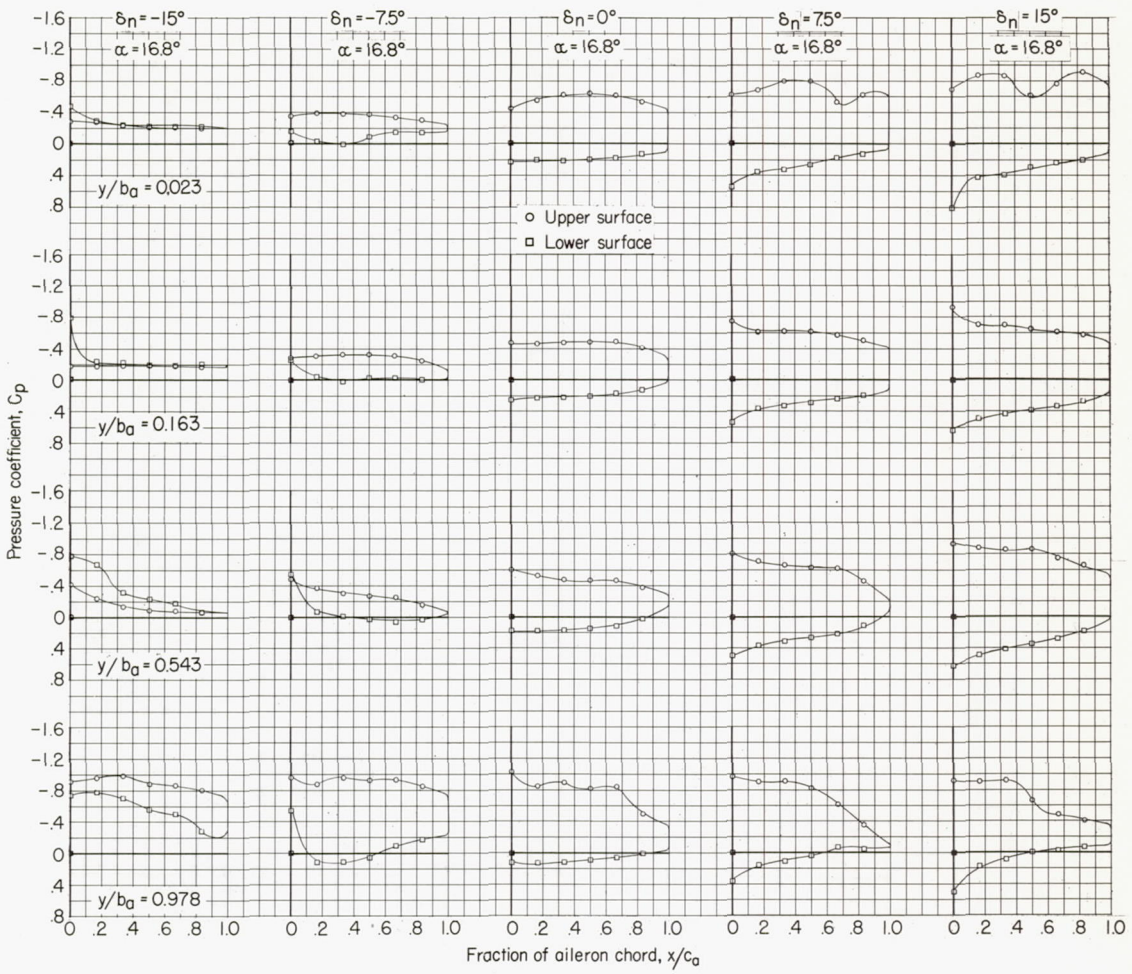

(e) $\alpha \approx 16.8^{\circ}$.

Figure 6.- Continued.

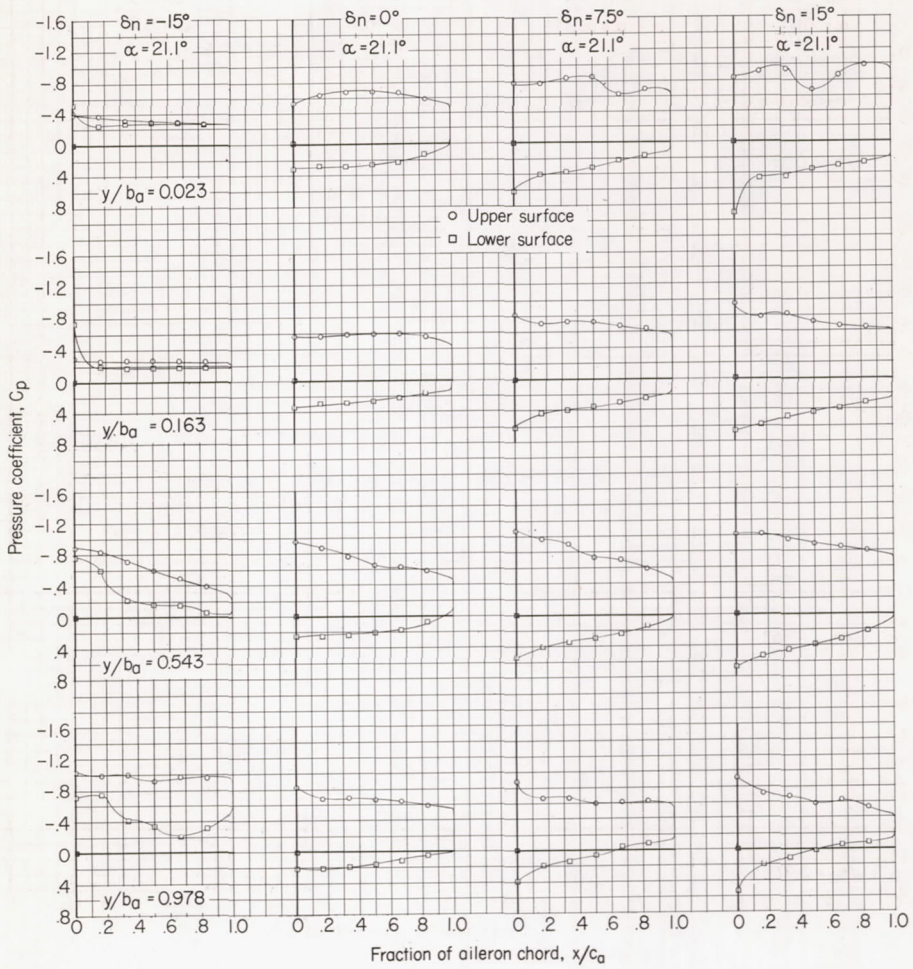

(f) $\alpha \approx 21.1^{\circ}$.

Figure 6.- Concluded.

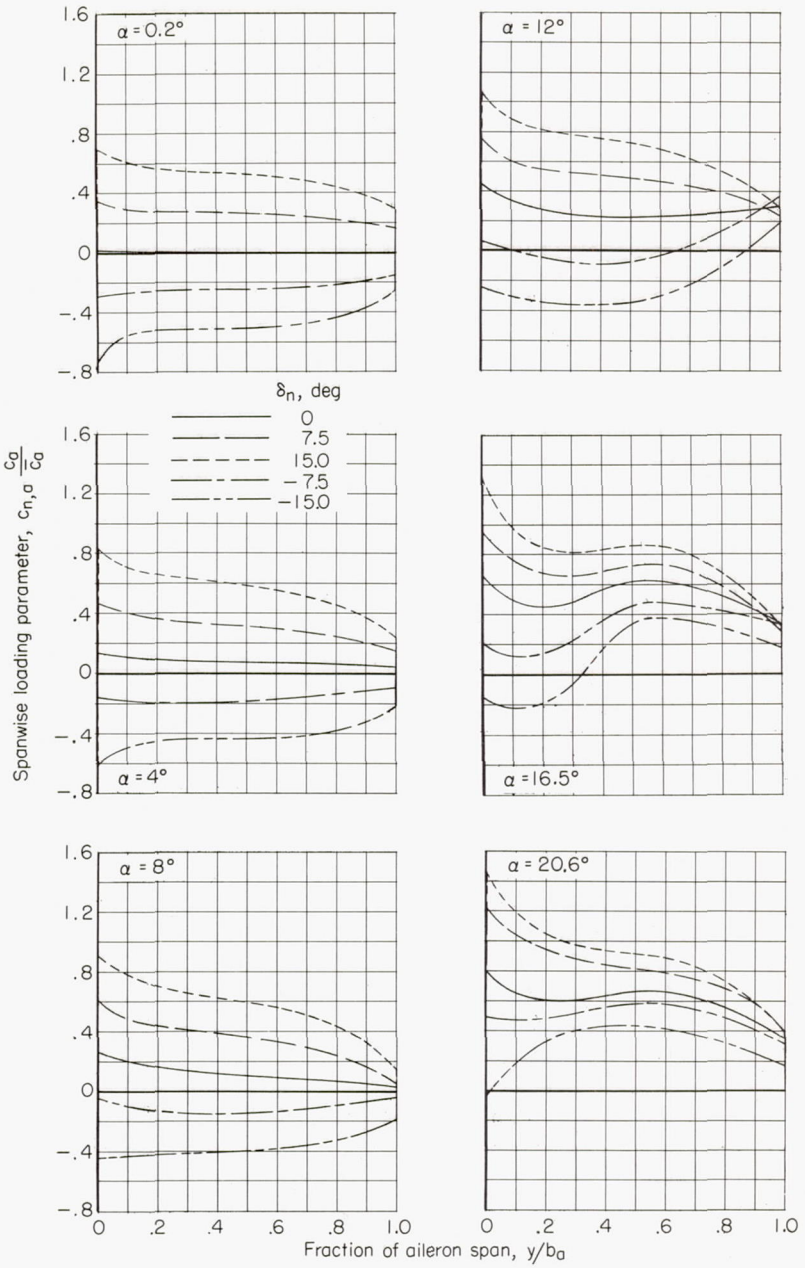

(a) M = 0.80.

Figure 7.- Spanwise loading over inboard aileron.

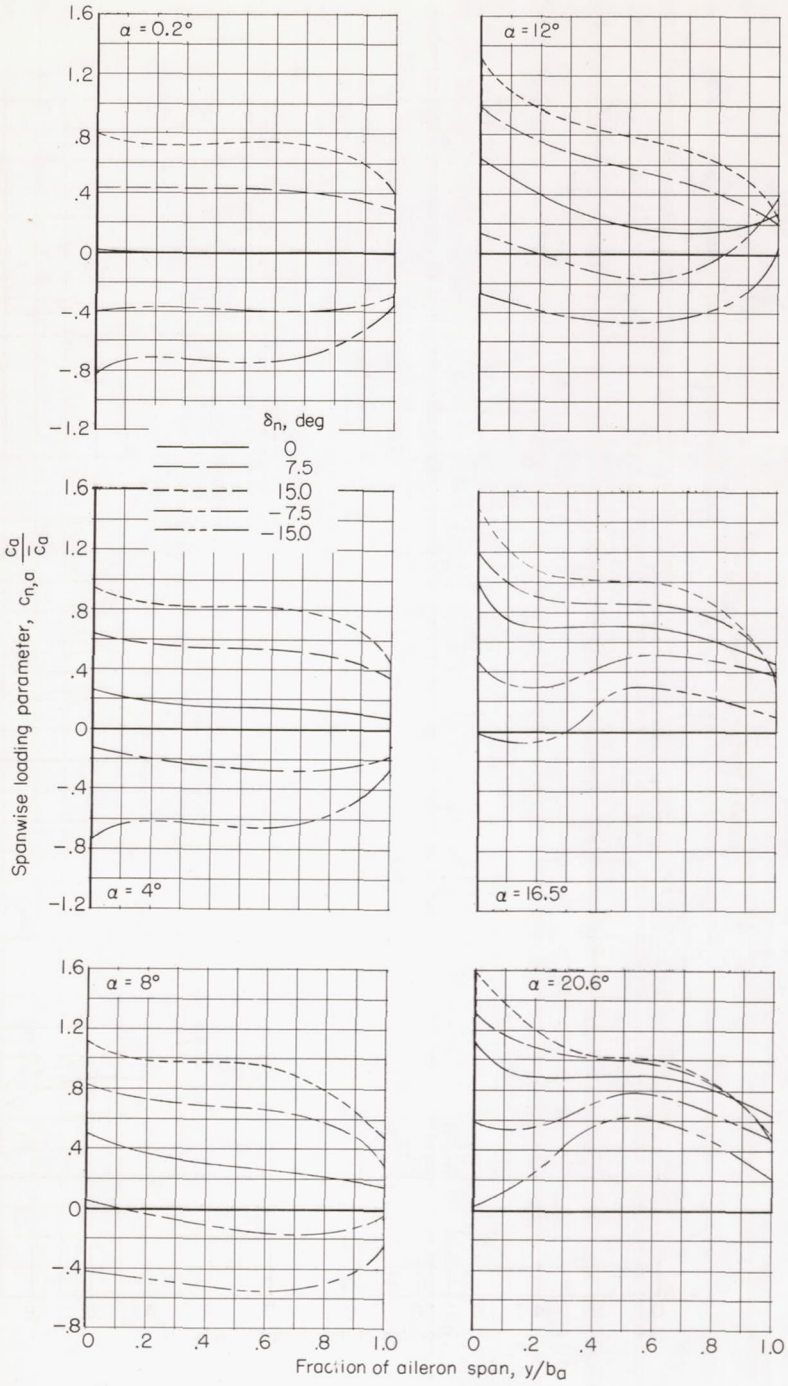

(b) M = 0.94.

Figure 7.- Continued.

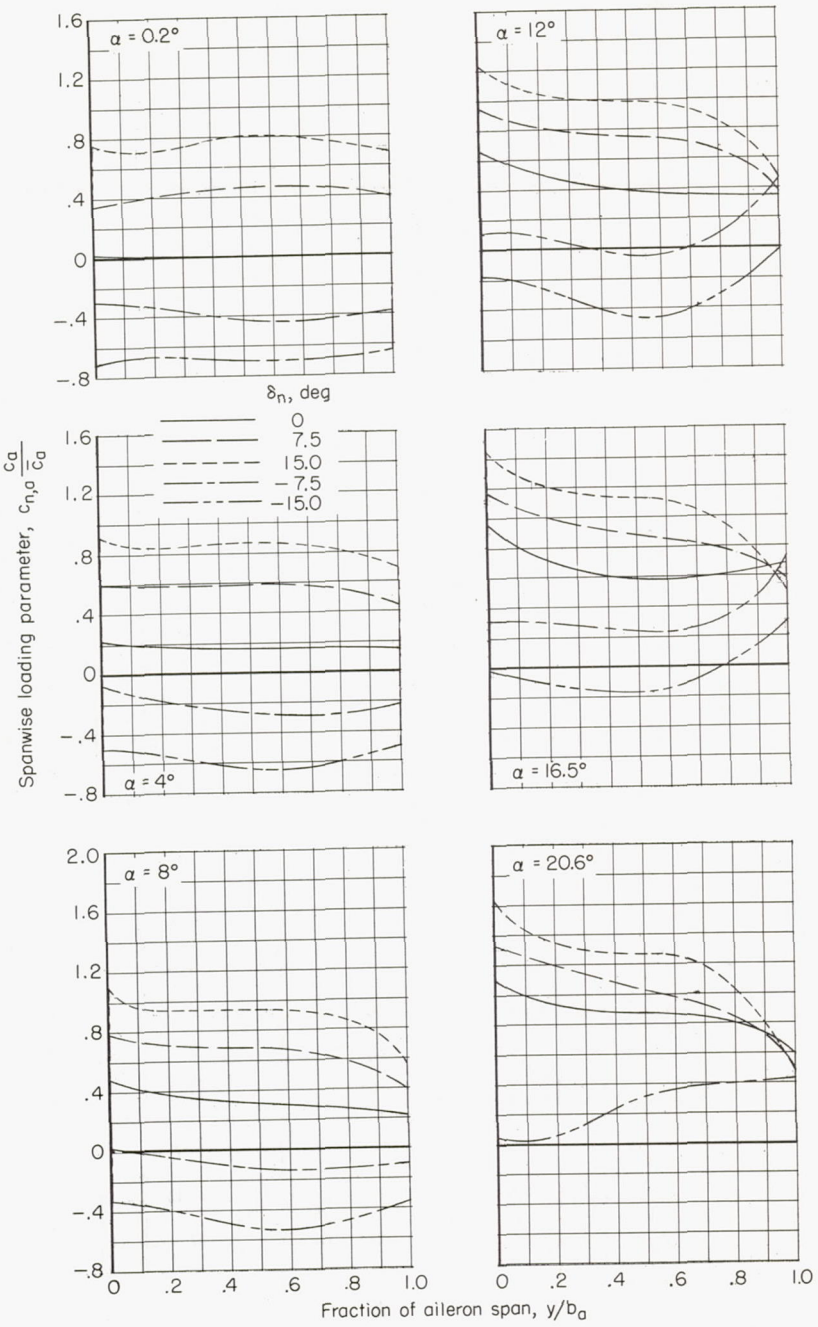

(c) M = 1.03.

Figure 7.- Concluded.

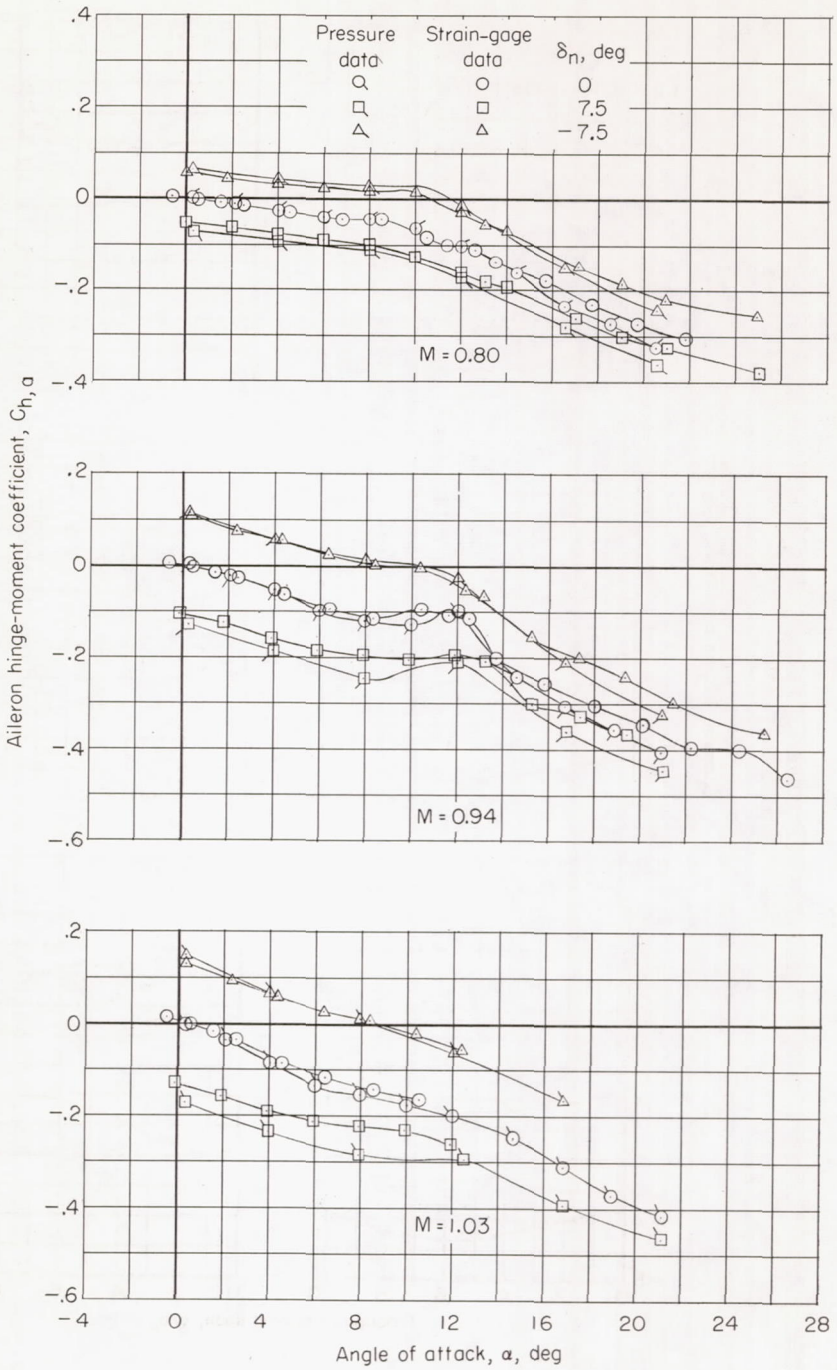

Figure 8.- Typical comparisons of aileron hinge-moment coefficients obtained from strain-gage-balance measurements and from pressure measurements. Inboard ailerons.

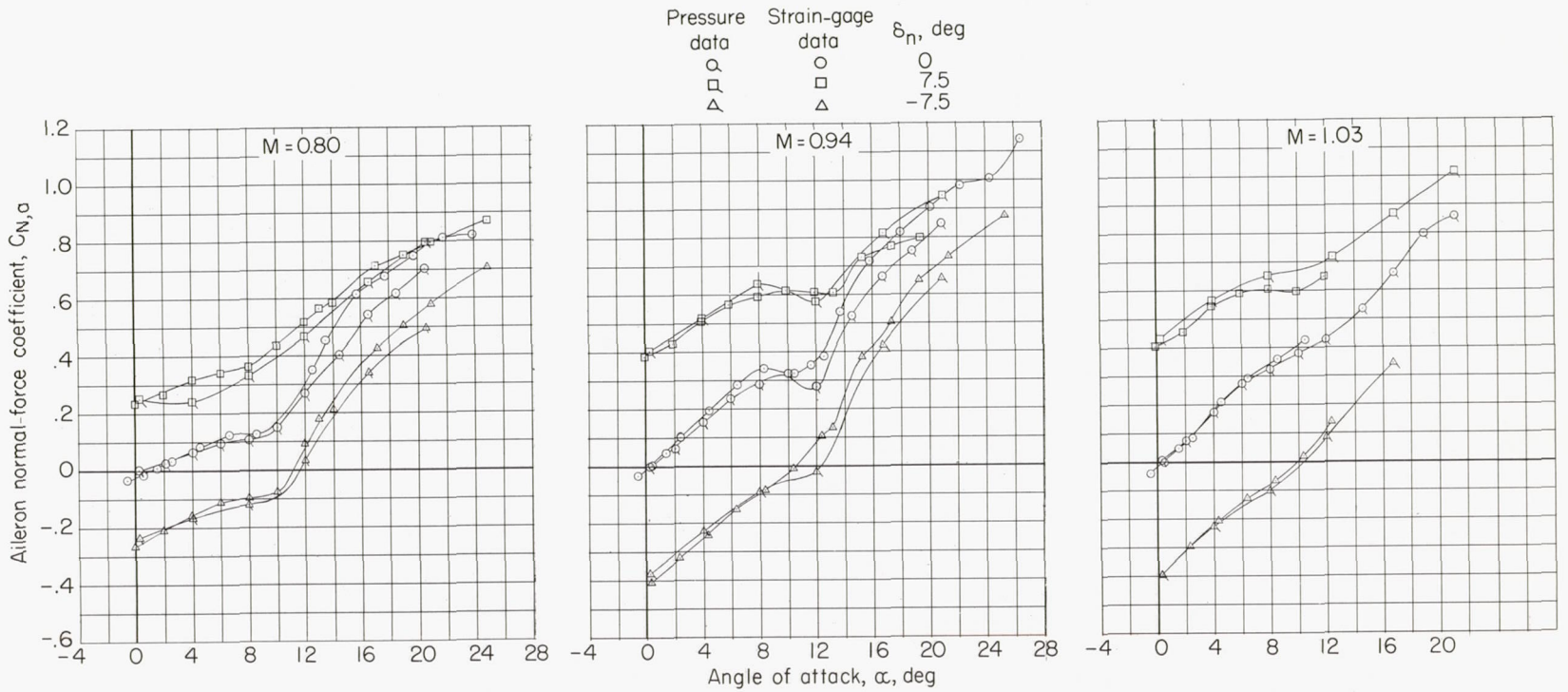

Figure 9.- Typical comparisons of aileron normal-force coefficients obtained from strain-gage-balance measurements and from pressure measurements. Inboard aileron.

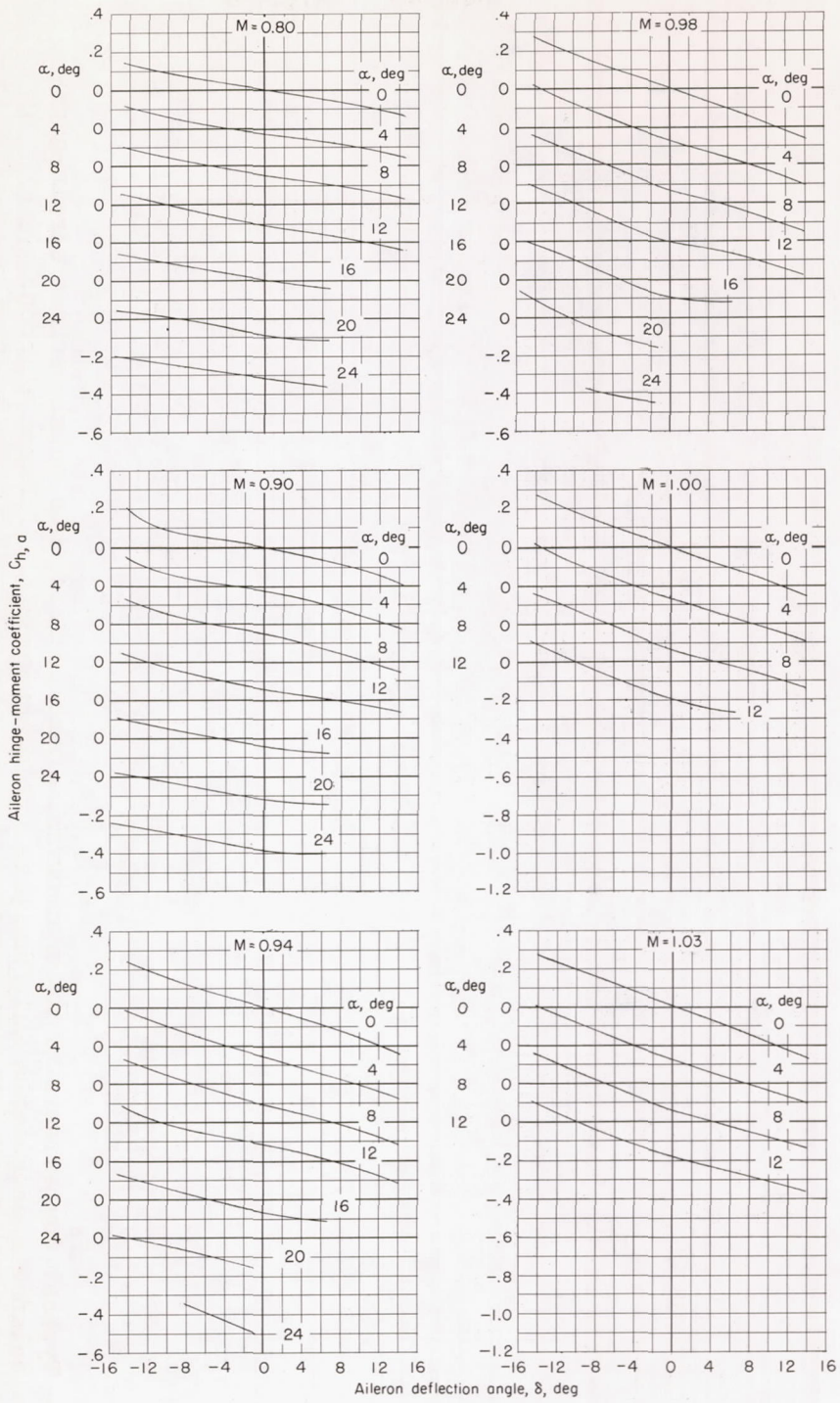

(a) Inboard aileron.

Figure 10.- Aileron hinge-moment characteristics as obtained from strain-gage-balance measurements.

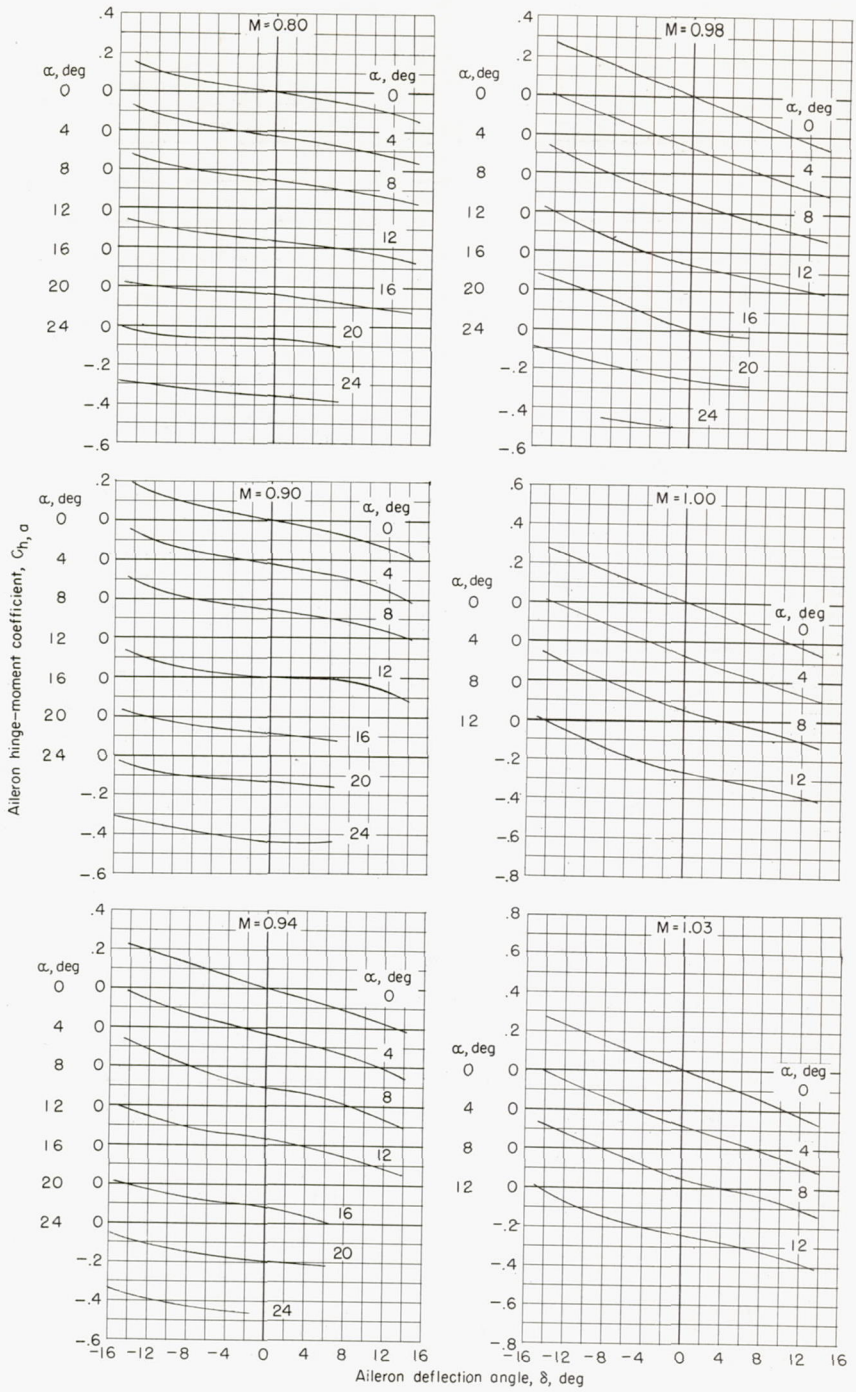

(b) Midspan aileron.

Figure 10.- Continued.

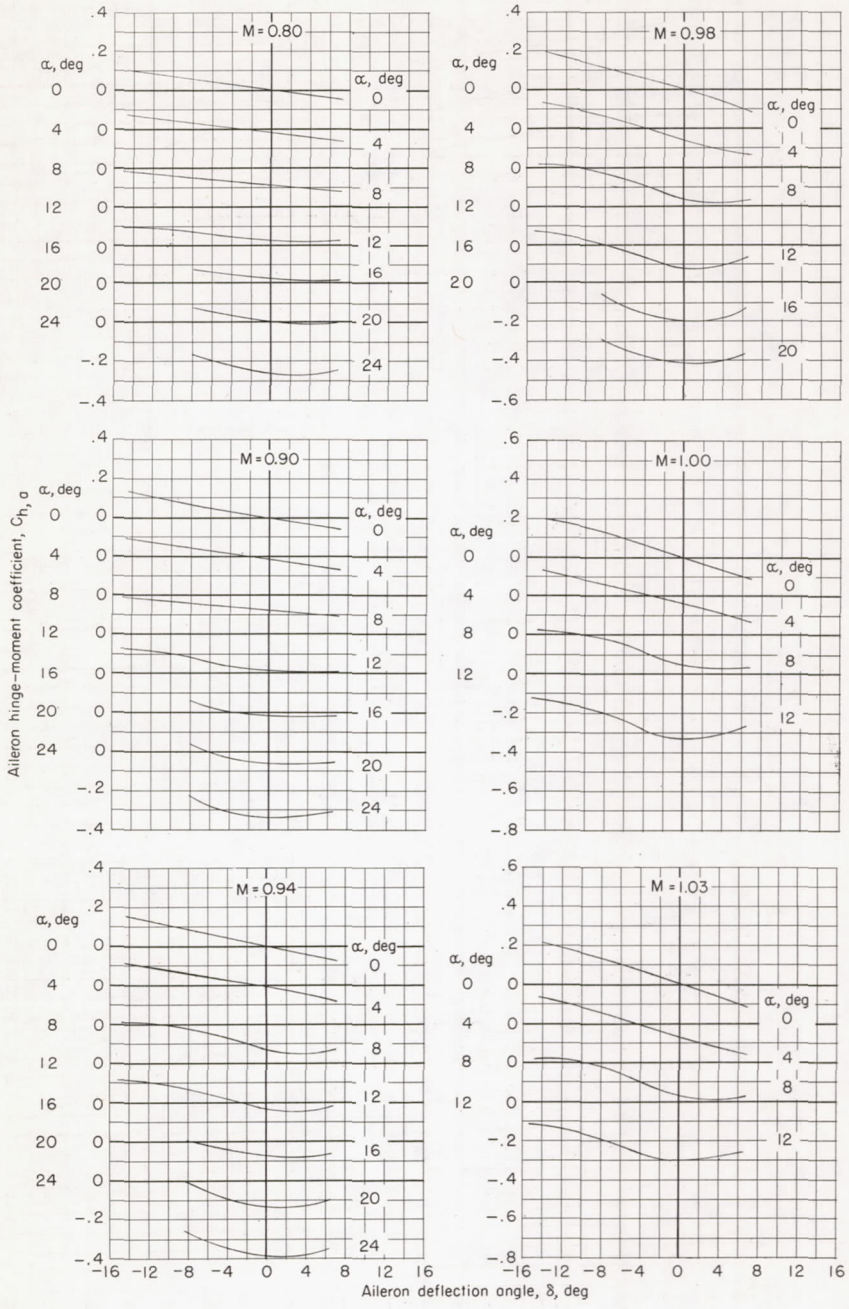

(c) Outboard aileron.

Figure 10.- Concluded.

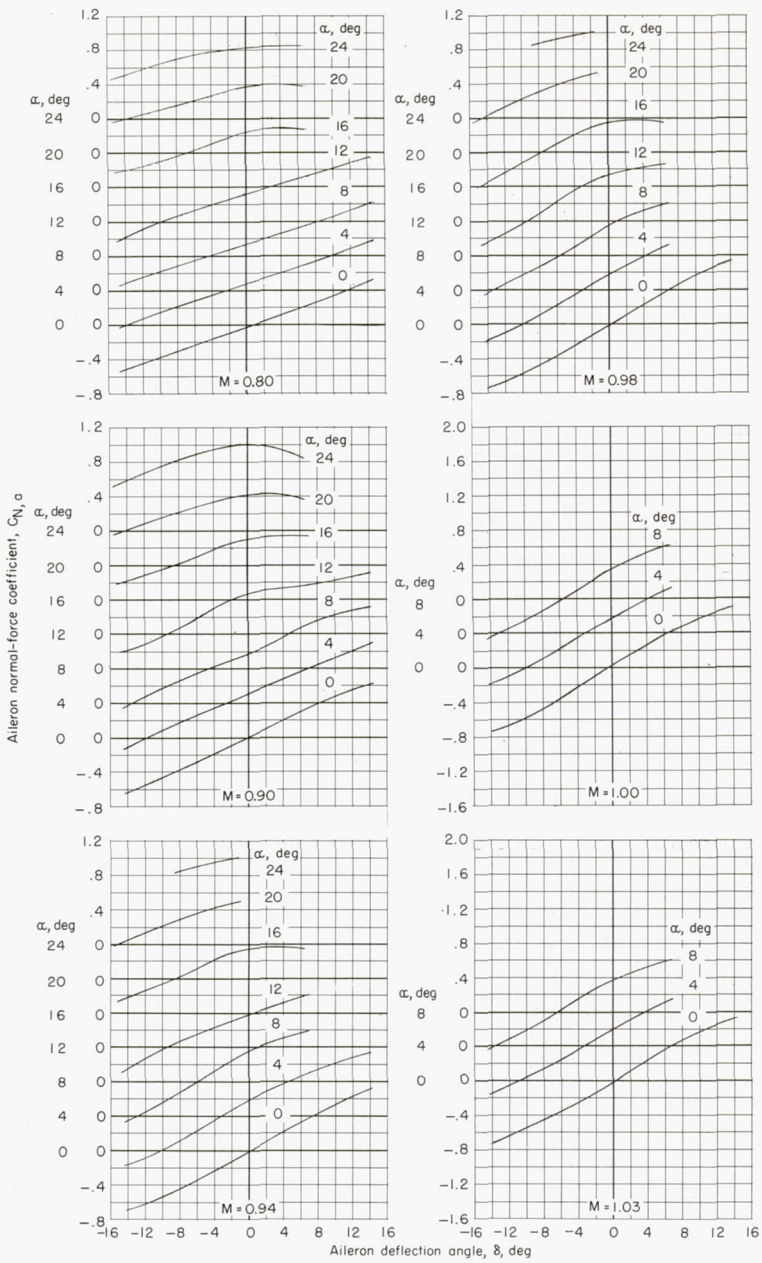

(a) Inboard aileron.

Figure 11.- Aileron normal-force characteristics as obtained from strain-gage-balance measurements.

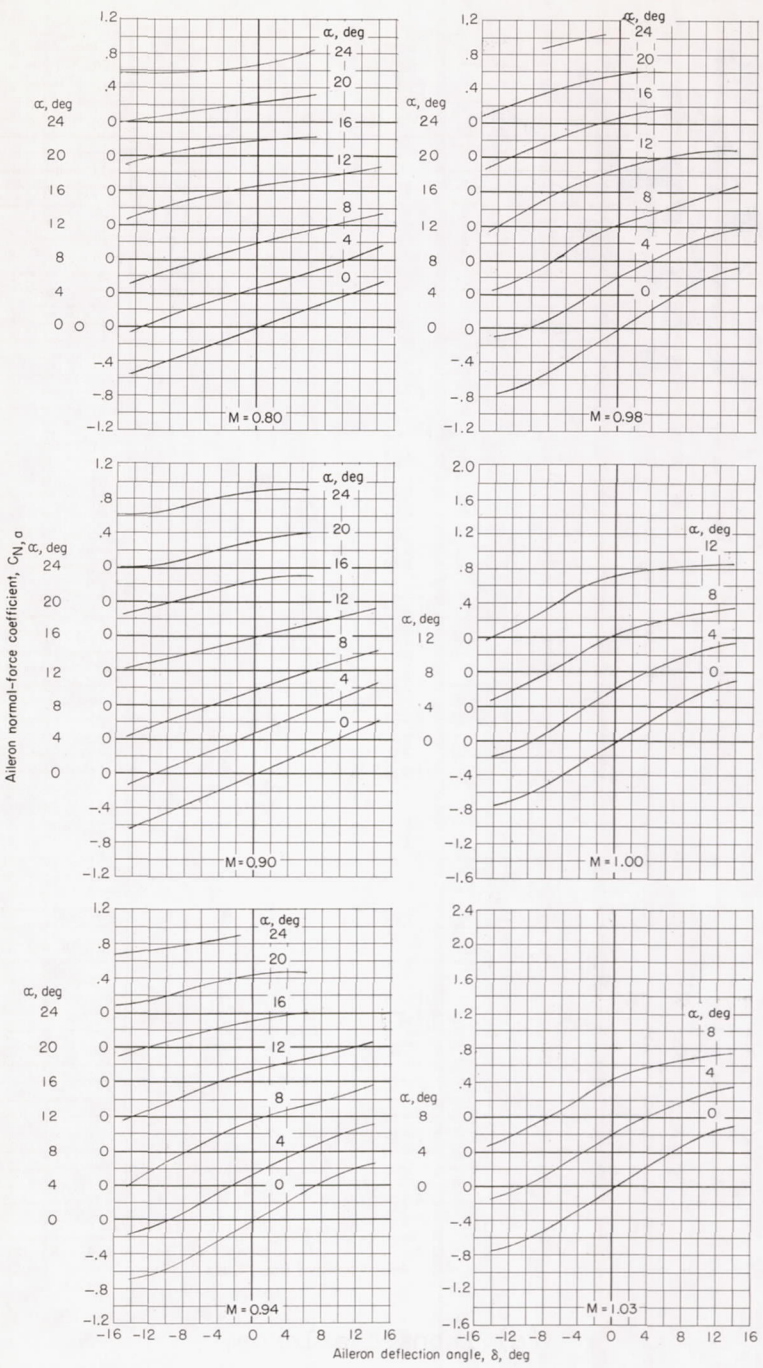

(b) Midspan aileron.

Figure 11.- Continued.

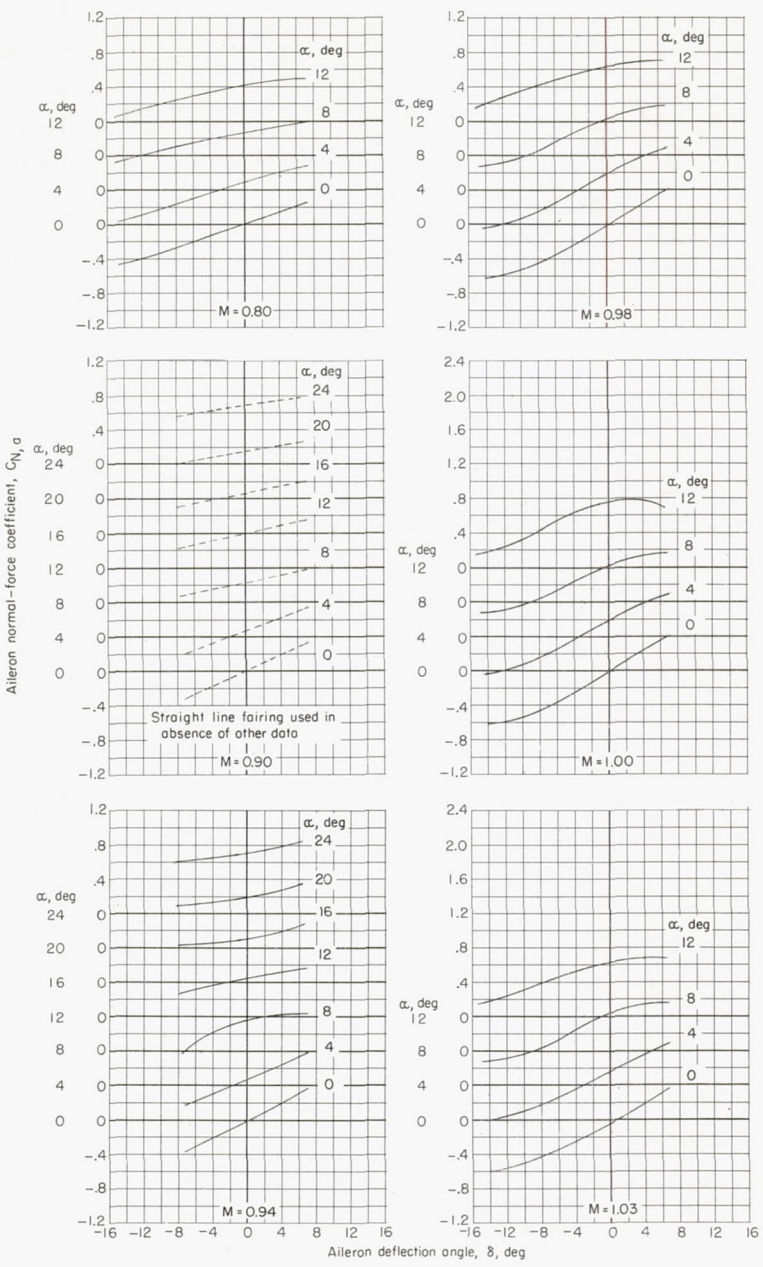

(c) Outboard aileron.

Figure 11.- Concluded.

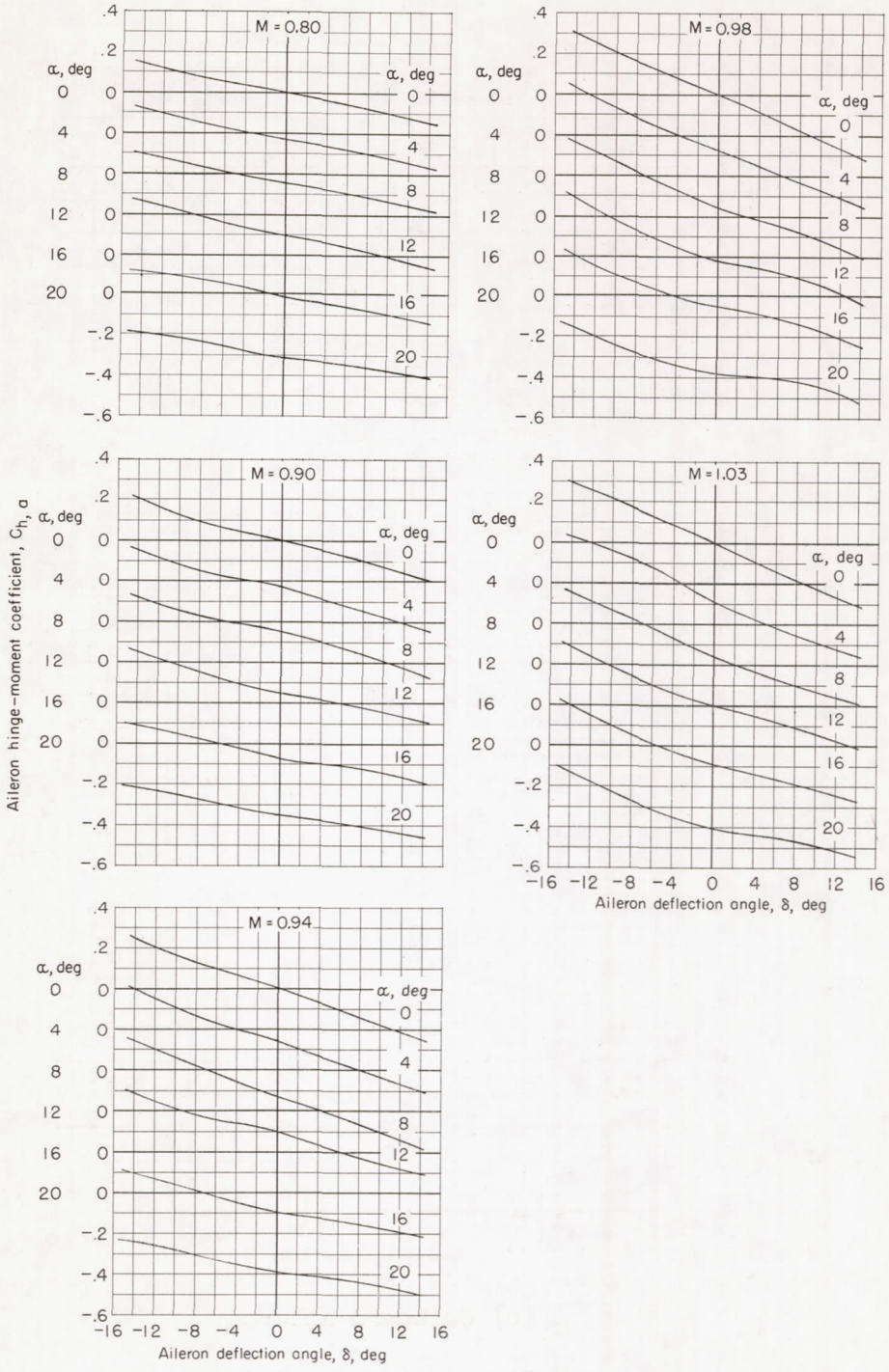

Figure 12.- Inboard-aileron hinge-moment characteristics as obtained from pressure measurements.

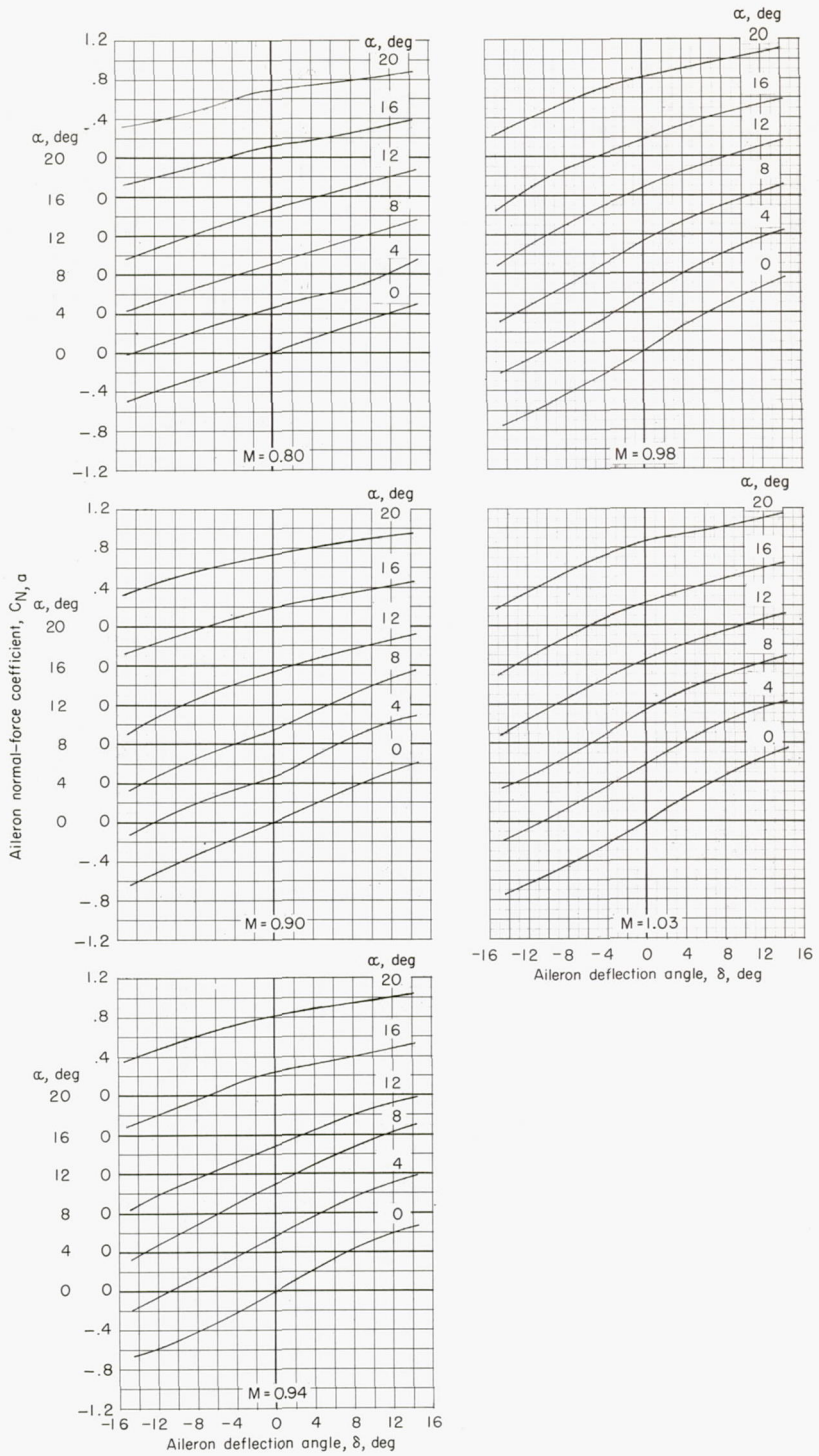

Figure 13.- Inboard-aileron normal-force characteristics as obtained from pressure measurements.

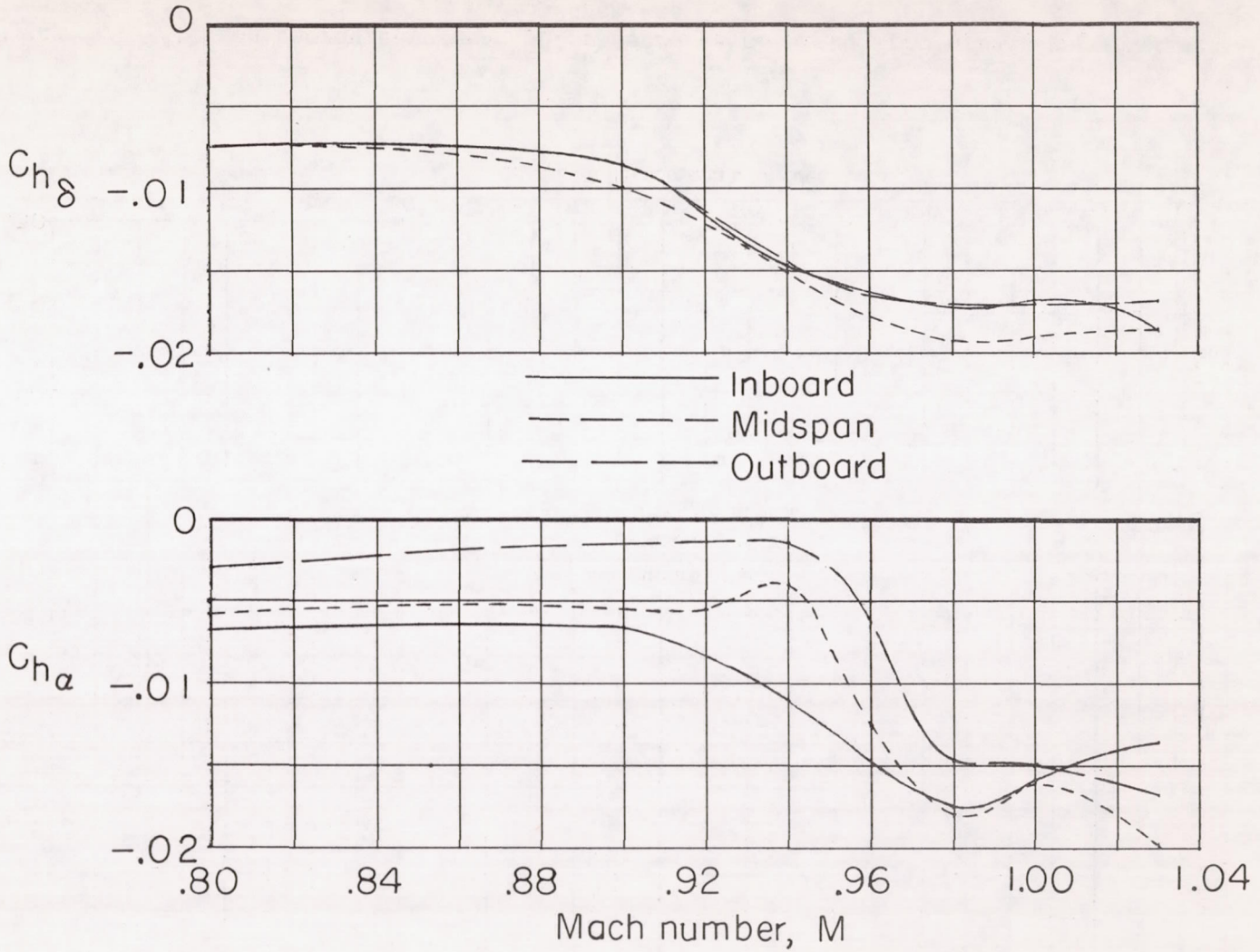

Figure 14.- Effect of Mach number on the parameters C_{h_δ} and C_{h_α} as obtained from strain-gage-balance measurements.

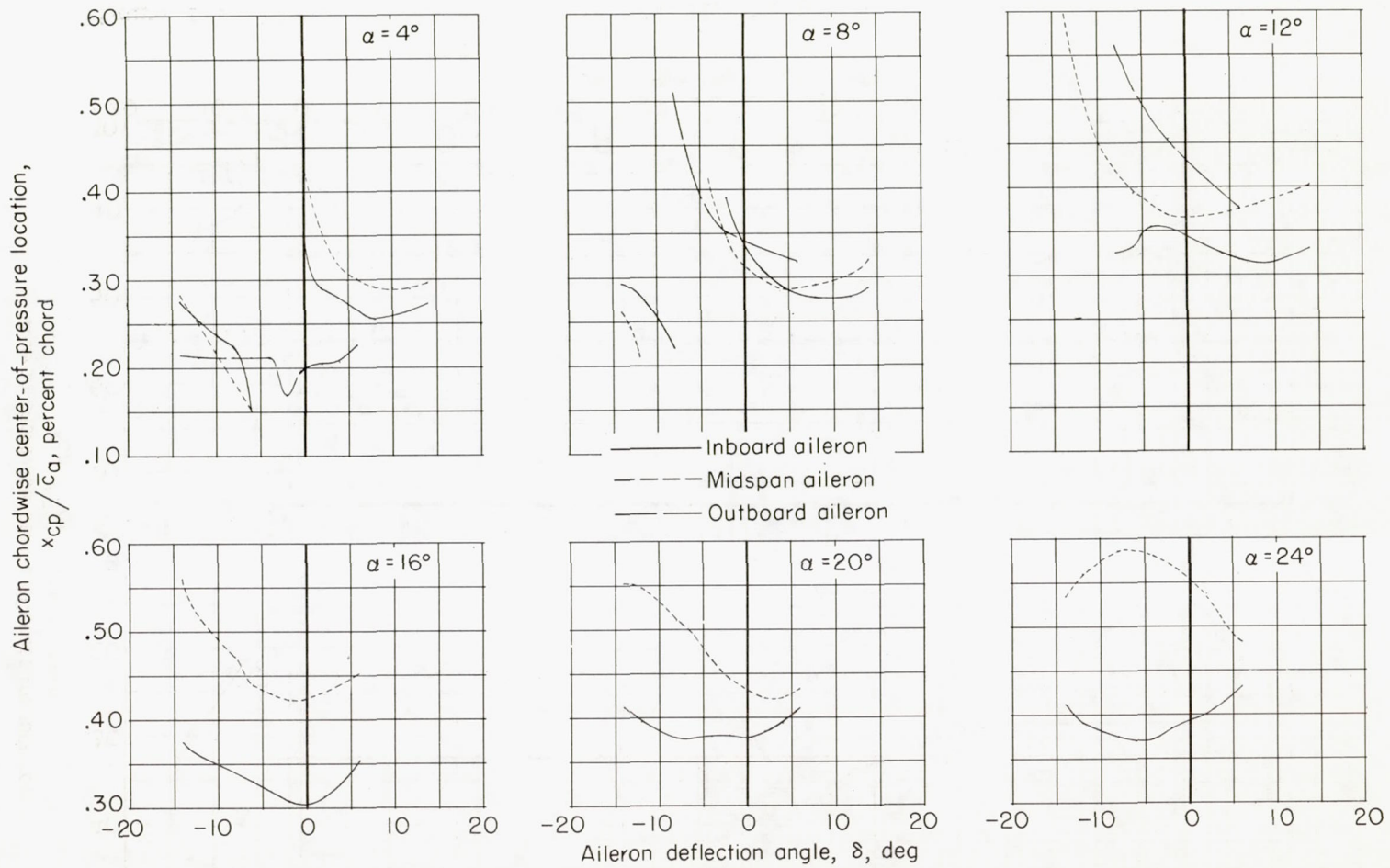

(a) M = 0.80.

Figure 15.- Aileron chordwise center of pressure as obtained from strain-gage-balance measurements.

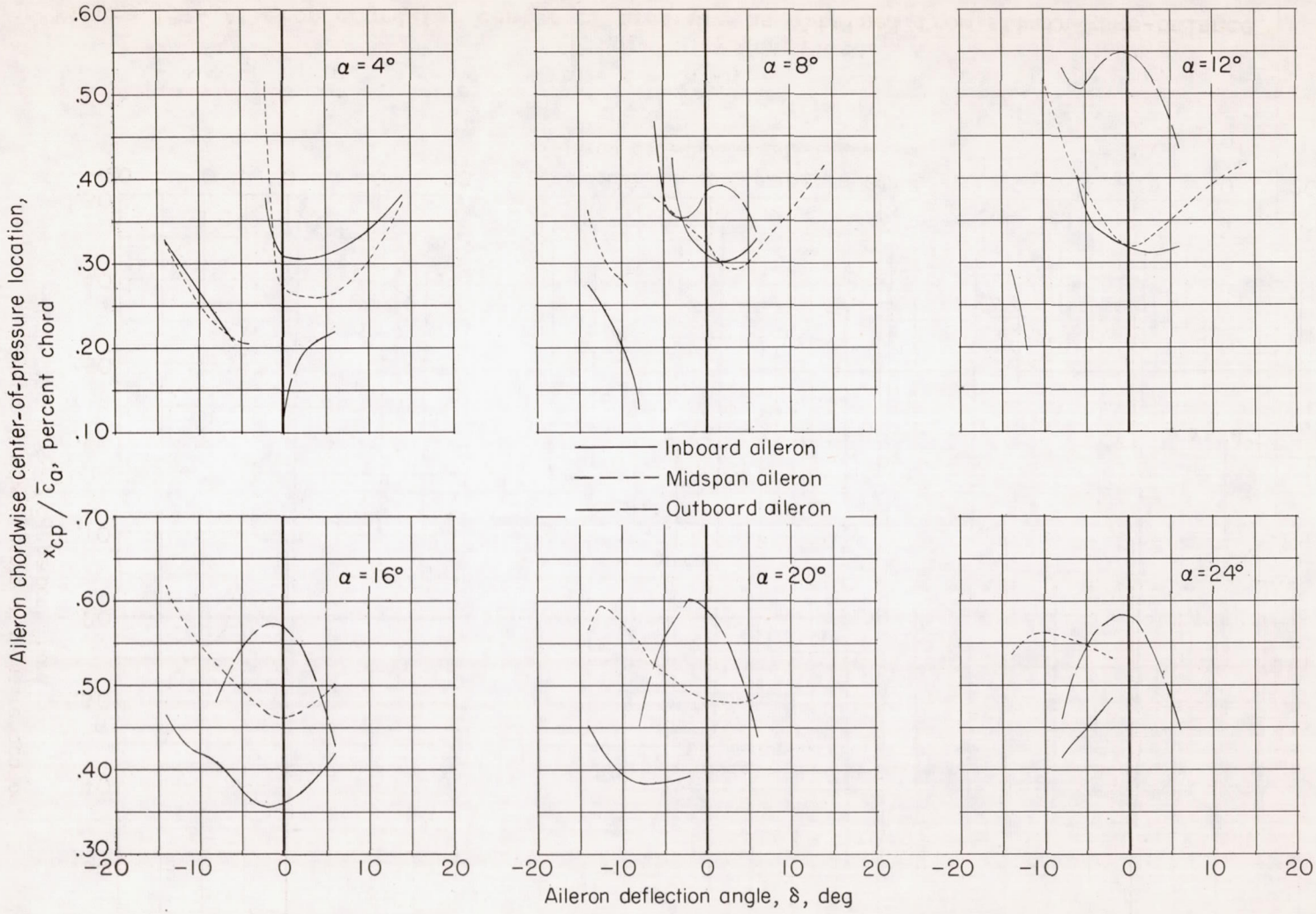

(b) M = 0.94.

Figure 15.- Continued.

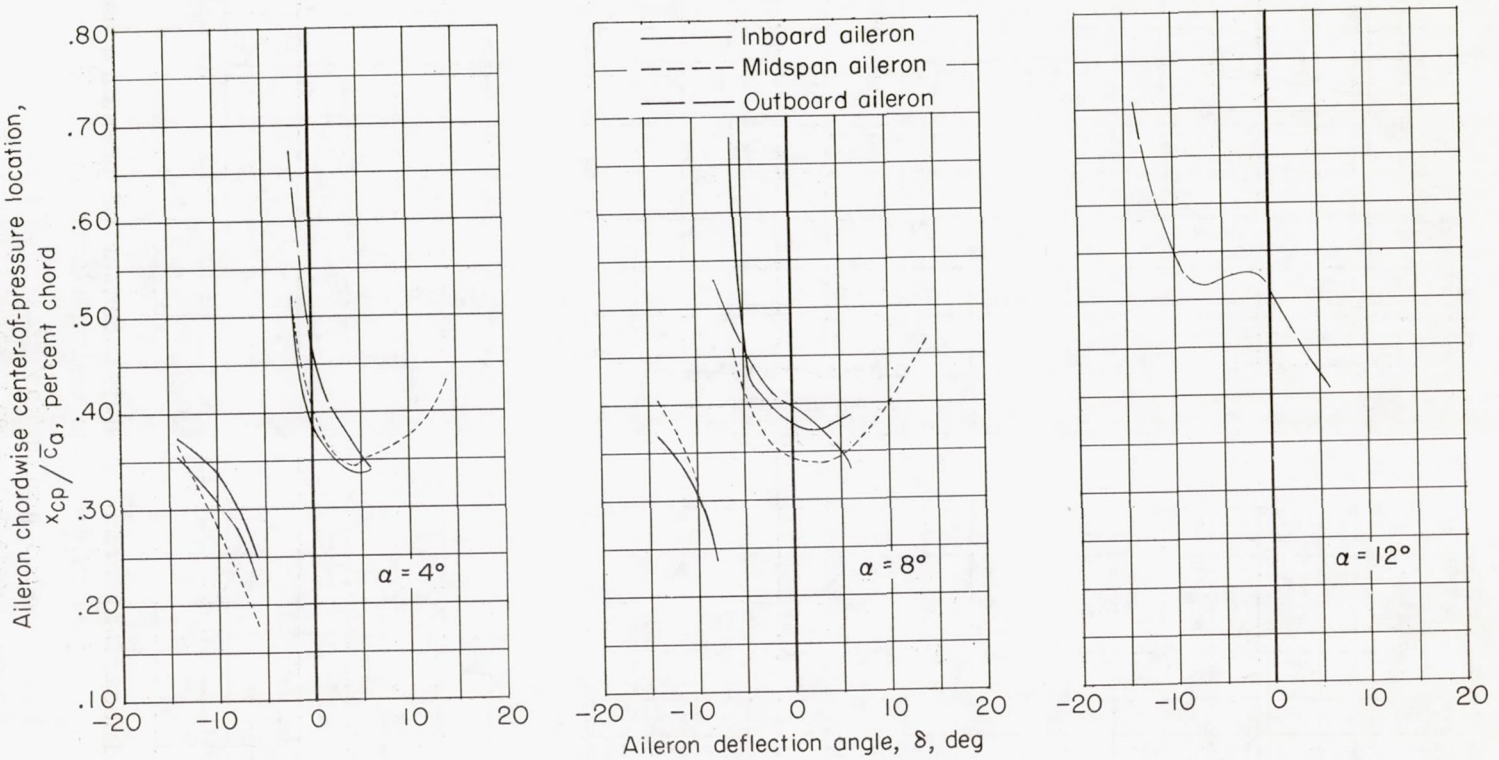

(c) M = 1.03.

Figure 15.- Concluded.

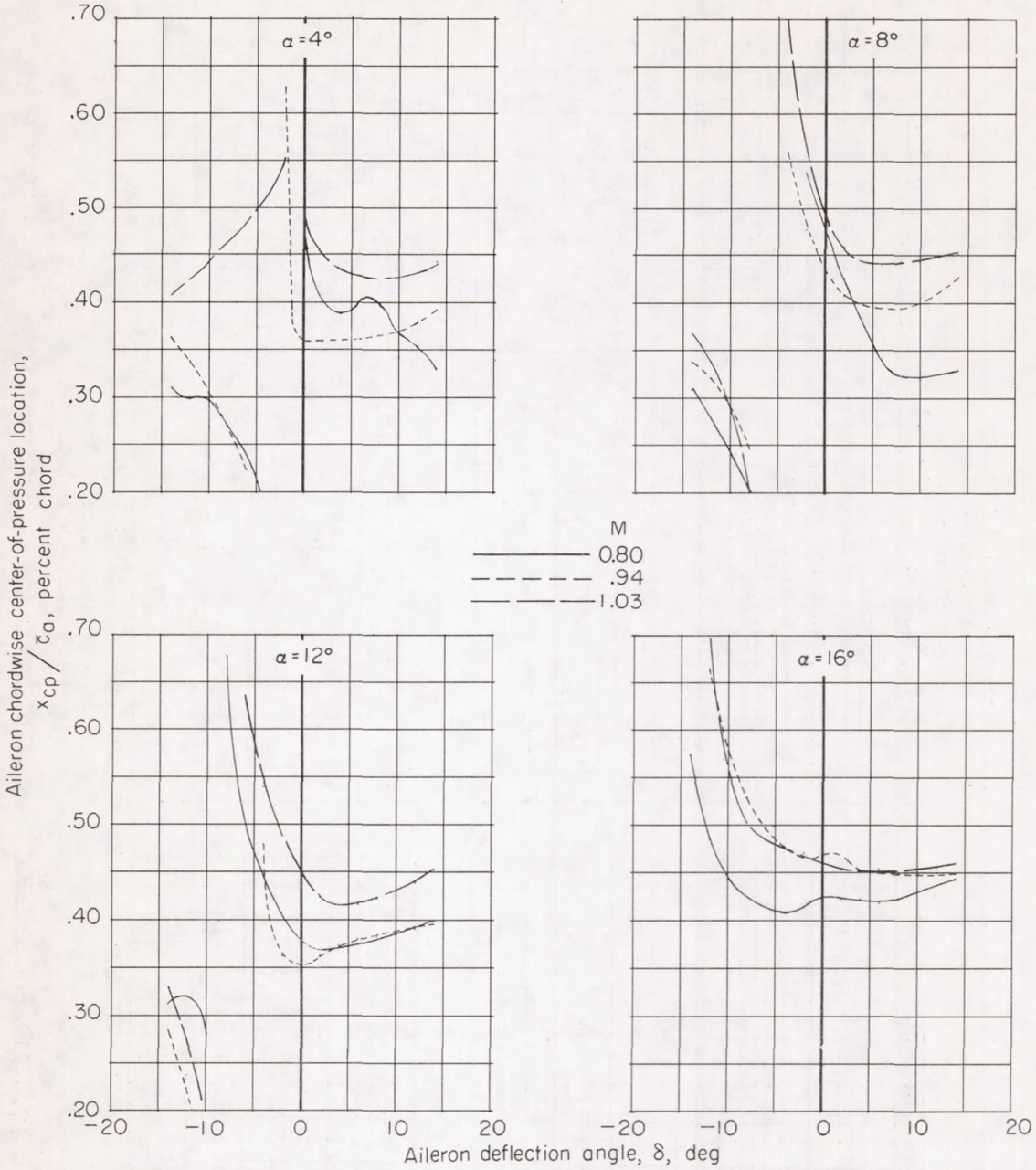

Figure 16.- Inboard-aileron chordwise center of pressure as obtained from pressure measurements.

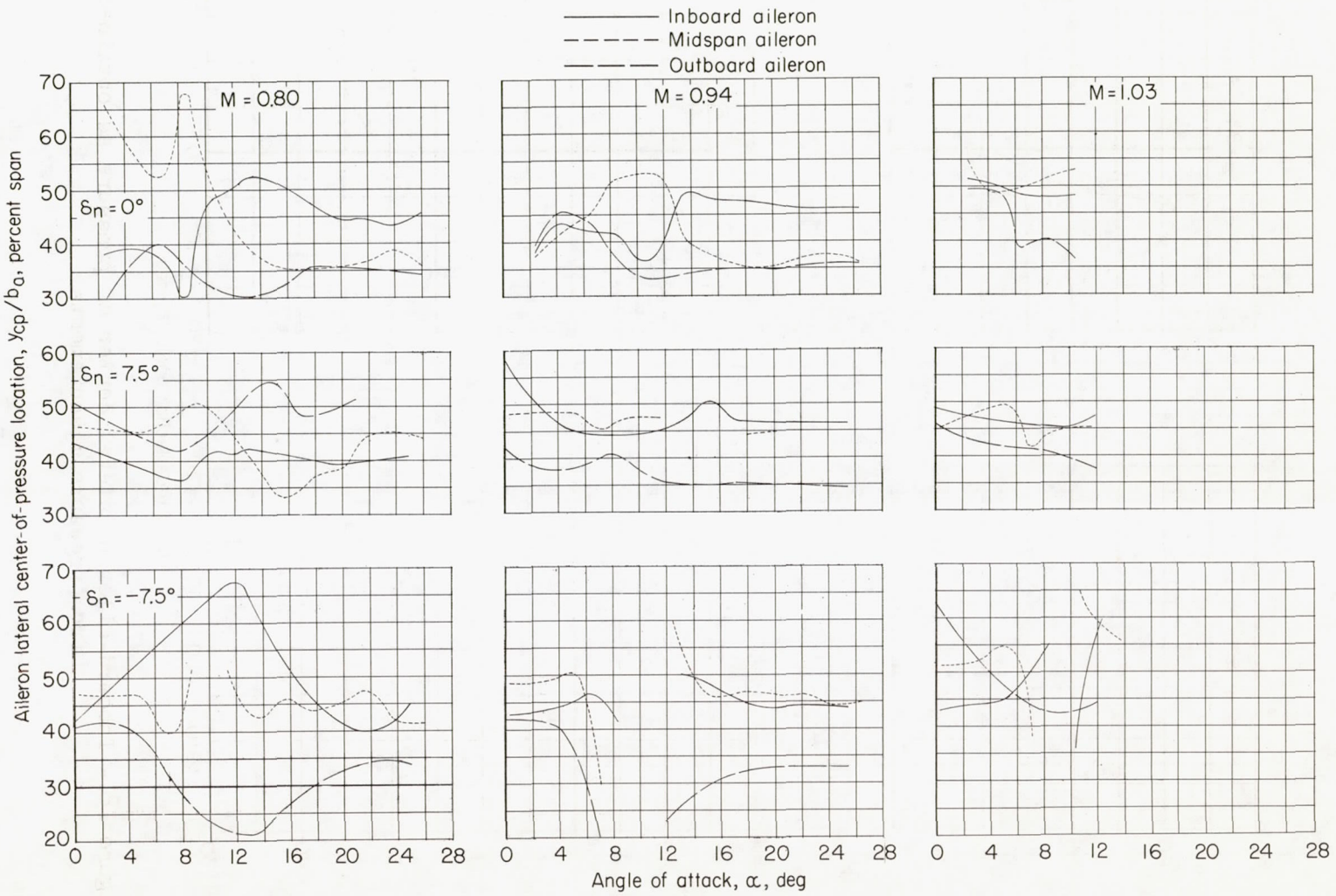

Figure 17.- Aileron lateral center of pressure as obtained from strain-gage-balance measurements.

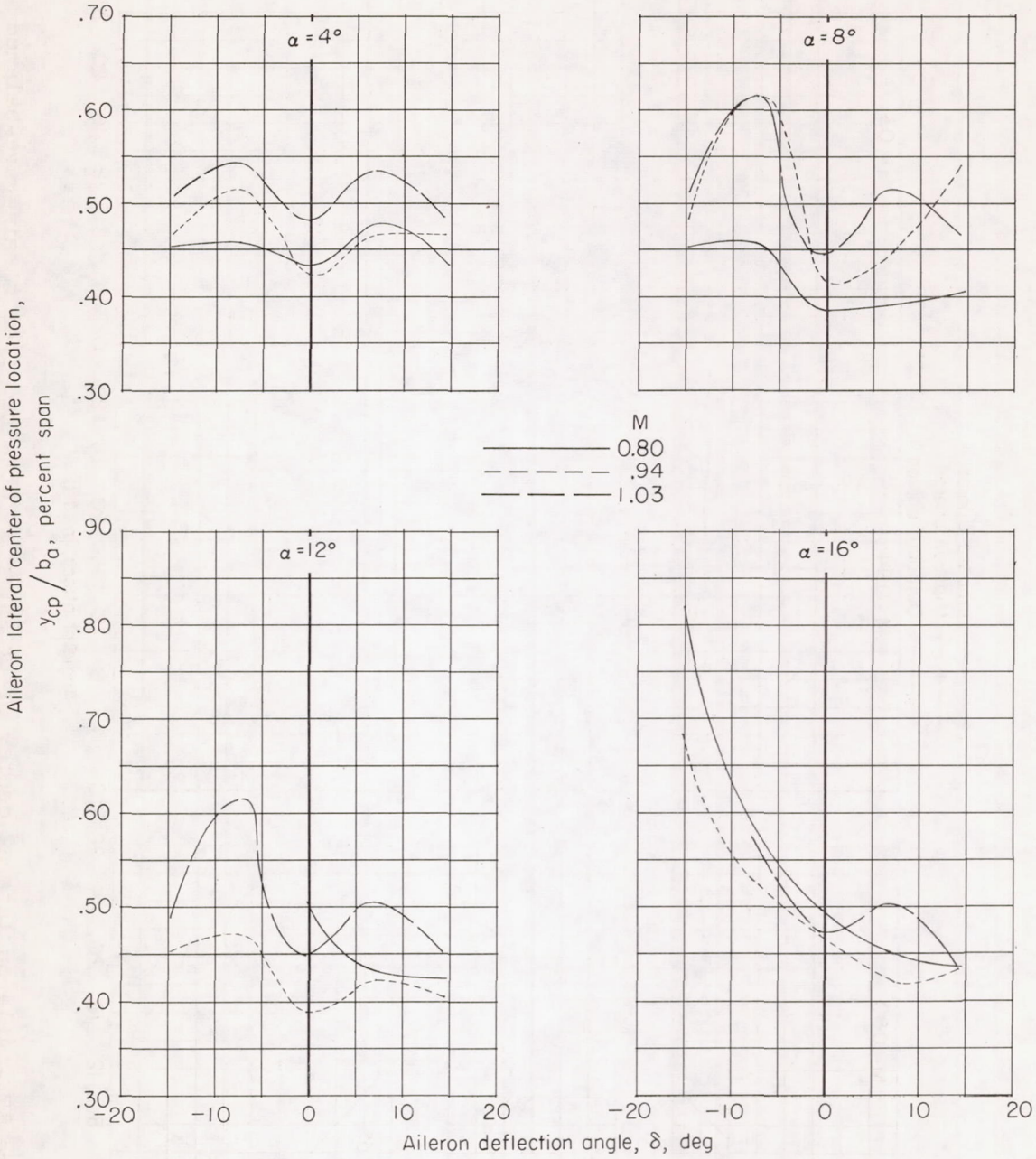

Figure 18.- Inboard-aileron lateral center of pressure as obtained from pressure measurements.